Accepted Manuscript

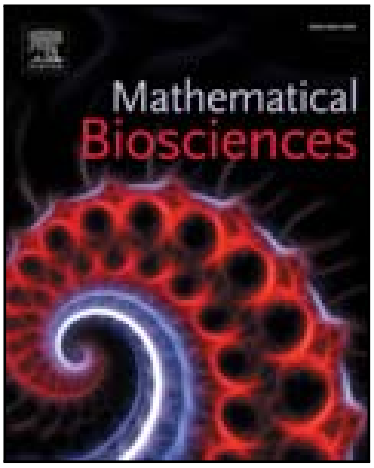

Anterior-Posterior patterning of Drosophila wing disc I: A baseline mathematical model

Zhan Chen, Yuting Zou

PII: S0025-5564(18)30060-9
DOI: https://doi.org/10.1016/j.mbs.2019.05.001
Reference: MBS 8208

To appear in: *Mathematical Biosciences*

Received date: 31 January 2018
Revised date: 3 May 2018
Accepted date: 8 May 2019

Please cite this article as: Zhan Chen, Yuting Zou, Anterior-Posterior patterning of Drosophila wing disc I: A baseline mathematical model, *Mathematical Biosciences* (2019), doi: https://doi.org/10.1016/j.mbs.2019.05.001

Highlights

- We proposed a baseline mathematical model that integrates established empirical facts to investigate the formation of pMad and Tkv gradients in both Anterior (A) and Posterior (P) compartments of Drosophila wing disc. To the author's best knowledge, this can be the first time that a mathematical model is used to study the morphogen Dpp signaling activity in both compartments.
- Our model can accurately regenerate complex experimentally-measured profiles of Tkv and pMad in both A and P compartments of wing disc.
- Parameter sensitivity was carried out to ensure that our results and conclusions are robust against specific choices of parameter values.
- Using the proposed model, we examined individual roles played by engrailed (En), Hedgehog (Hh) and Dpp in the establishment of Tkv and pMad profiles. That is not an easy task for the experimentalist. By doing so, the model sheds some light on the underlying mechanisms of the AP patterning. Meanwhile, our validated model can be considered as a starting point for further studies of other players and their roles in the AP patterning and growth.

Anterior-Posterior patterning of Drosophila wing disc I: A baseline mathematical model

Zhan Chen and Yuting Zou
Department of Mathematical Sciences
Georgia Southern University, Statesboro, GA

May 11, 2019

Contents

I Introduction **2**

II Model and computational methods **5**
II.A The mathematical model 5
II.B Parameter estimate 8
II.C Other computational setting 8

III Computational results and discussions **9**
III.A Validation 9
III.A.1 Dpp signaling 9
III.A.2 Another validation by Tkv mutation and Dpp overexpression 11
III.A.3 Overshoot of Hh and its signaling 11
III.B Specific roles of individual components on the Tkv and pMad patterning 12
III.B.1 Upregulation of Tkv by En in the P compartment 14
III.B.2 Hh repressing Tkv in Hh signaling cells 14
III.B.3 Downregulating Tkv by Dpp 14
III.C Parameter sensitivity and robustness 17

IV Conclusion **18**

V Appendix **20**
V.A Proof that gene *tkv* expression level is proportional to the level of total Tkv proteins 20
V.B Parameters estimation 20
V.B.1 Parameters involved in the Hh module 20
V.B.2 Parameters in the Dpp module 21

Abstract

Wing imaginal disc of Drosophila is one of the commonly used model systems for the studies of patterning, growth, and scaling. Development of the wing disc involves many interacting components as well as a variety of compound processes whose underlying mechanisms are still under investigation. For instance, it remains unclear about how to form compound experimentally-measured patterns of Decapentaplegic (Dpp) type-I receptor Thickveins (Tkv), as well as phosphorylated Mothers Against Dpp (pMad) which is the indicator of Dpp signaling activities. In this work, we proposed a baseline mathematical model that integrates established experimental facts to investigate the formation of pMad and Tkv gradients. Our model is validated by the accurate reproduction of complex asymmetric profiles of Tkv and pMad in both anterior and posterior compartments of wing disc. Moreover, using our model

as a numerical platform, we examined specific roles played by engrailed (En), Hedgehog (Hh) and Dpp in the establishment of Tkv and pMad profiles. It turns out that all En, Hh, Dpp play an essential role in the formation of pMad and Tkv patterns. In particular, our proposed model supports the crucial part of the downregulation of Tkv by Dpp. Besides, dual negative regulations of Tkv by both Hh and Dpp simultaneously prevent the Dpp signaling from interfering and expand the effective range of Dpp gradients. Finally, parameter sensitivity was carried out to ensure that our results and conclusions are robust against specific choices of parameter values.

Key words: Drosophila wing disc, Dpp, pMad, Anterior-Posterior patterning, mathematical model.

I Introduction

Drosophila, the common fruit fly, is one of the most widely used model organisms in biology because of its short life cycle, high reproduction rate, and genetic tractability aided with well-developed molecular techniques.[1] It has been discovered that signal transduction and gene networks, which control patterning and growth in Drosophila, are highly conserved across various species, and nearly 75% of human disease-associated genes are believed to have a functional homology in the fly.[2] As such, a better understanding of the underlying mechanisms that control developmental processes in Drosophila may deepen our understanding of similar processes in other organisms including humans, and then further our knowledge for the treatment of diseases such as cancer and birth defects. In particular, the wing imaginal disc (wing disc) of Drosophila is one of the commonly adopted model systems for the studies of patterning and growth which are two fundamental problems in developmental biology. Although many signal transduction networks have been known in the Drosophila wing disc, it is still unclear how these networks interact and cooperate to generate observed spatiotemporal patterns of gene expression, and how overall phenotypes of organs such as the wing are controlled.

Wing discs of Drosophila can be divided into anterior (A) and posterior (P) compartments (See Figure 1) by the selector gene engrailed (En). En, solely expressed in the cells of P compartment, plays a tremendous role in the anterior-posterior (AP) signaling process. It is a transcription factor that identifies cells in the P compartment and changes cell surface properties.[1,3,4] As a result, the boundary between A and P compartments (AP boundary) is established. The AP boundary is defined early in the embryo and maintained throughout the larval stages. Moreover, the En expression in the P compartment autonomously induces the expression of Hedgehog(Hh), a short-range morphogen that is central to the AP patterning of Drosophila wing disc.

The Hh signaling pathway is one of the most important pathways that have been extensively studied for the patterning of wing disc. Ligand Hh is secreted exclusively from cells of the P compartment under the control of En. After its secretion, Hh diffuses to the A compartment and forms a concentration gradient. In the A compartment, Hh induces several target genes such as dpp and ptc (See Figure 1) by binding with its receptor Patched (Ptc), as it was observed that the Hh signaling activity depends on the ratio of bound to free Ptc.[3,5,6] In addition, Hh signaling upregulates the ptc transcription.[5,6] This feedback gives Ptc the dual functions of both receiving the signal of Hh and limiting the spread of Hh in the A compartment.

One of the target genes activated by Hh is gene decapentaplegic (*dpp*) which is a member of the Bone Morphogenetic Protein (BMP) subfamily (See Figure 1). The Dpp signaling pathway is another pathway that is essential for both patterning and growth in the wing disc,[1,3] and it is conserved across organisms. Ligand Dpp is expressed and secreted in a stripe of anterior cells adjacent to the AP boundary. After their secretion, Dpp molecules transport and form a concentration gradient which determines cell fates in the concentration-dependent manner (See Figure 1).[4] There are a variety of possible mechanisms for the Dpp transport including diffusion, endocytosis, and transcytosis or bucket brigades.[9,10] Among these, the diffusive mechanism, coupled with the uptake by cell-surface receptors and subsequent degradation, seems to be quite plausible and supported by increasing evidence.[10,11] Through Dpp preferentially binding with a type-I receptor Thickveins (Tkv), the local extracellular concentration of Dpp is converted into the intracellular gradient of phosphorylated Mothers Against Dpp (pMad) which is considered as the sole known transmitter of Dpp-Tkv activity to regulate its downstream target gene expressions.[11,12]

Moreover, it is evident that Dpp plays a necessary role in the growth of wing disc.[1] For example, ubiquitous Dpp expression results in disc overgrowth,[13] and flies that lack the Dpp expression in the

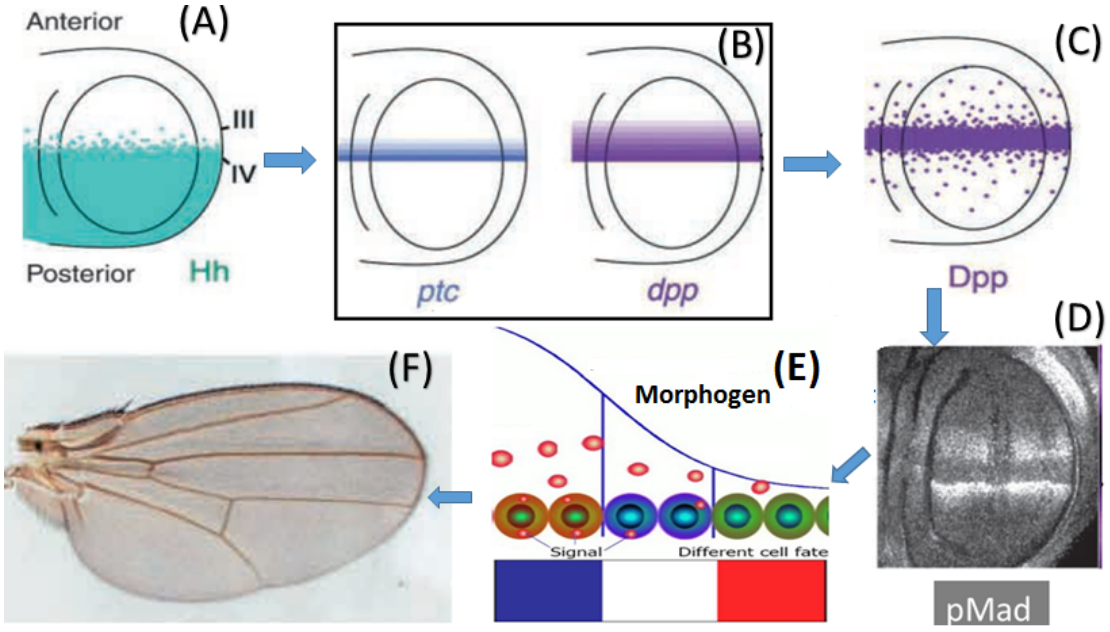

Figure 1: **The wing is controlled by morphogen Dpp and explained with French flag model** . Short-range Hh, ubiquitously generated in the posterior compartment, diffuses to the anterior compartment to form a gradient in a strip of cells adjacent to the AP boundary in the A compartment (See (A)). This leads to the induction of gene *ptc* and *dpp* in the strip (See (B)). Ligand Dpp is secreted in the strip of cells adjacent to the AP boundary and then transport in the wing disc (See (C)). Meanwhile, Dpp binds to its receptor to phosphorylate Mothers Against Dpp (pMad) (See (D)). Consequently Dpp signaling determines the cell fates through morphogen gradients based on French flag model (See (E)).[7,8] Finally, cell fates are reflected by wing phenotypes (size, veins etc see (F)). This figure is produced with sub-pictures taken from Tabata et al[3] and.[7] Here the wing disc is simplified into a 2D cartoon domain and is divided into anterior and posterior compartments.

wing disc fail to form wings.[14] Additionally, as the wing disc grows, Dpp and its activity gradient scale with the tissue size.[1] Both Dpp gradient and its cellular response (visualized by pMad antibodies) expand and adjust to the growing tissue size.[11,15] However, how Dpp coordinates patterning and growth during development remains unknown.[11]

As described above, Dpp type-I receptor Tkv is essential for the Dpp signaling in the wing disc. This was confirmed by facts that eliminating *tkv* function leads to the absence of pMad while ubiquitous expression of *tkv* elevates pMad everywhere in the disc and causes disc overgrowth.[12] The profile of *tkv* expression shows an intricate pattern in the wing disc[3] which can be seen in Figure 2 (C) and (D) . It displays the lowest *tkv* level in cells of the Hh signaling region, and the *tkv* level gradually gets higher away from the AP boundary in the A compartment. It increases sharply in the cells abutting the AP border before a much slower increase toward the periphery area in the P compartment. Moreover, the level of *tkv* expression is higher in the P compartment than that in the A compartment. It has been postulated that the *tkv* distribution is dynamically regulated by En, Hh and Dpp. In particular, It was found that both Hh and En act through master of thickveins (Mtv), a transcription factor, to control the *tkv* expression.[12,16] En positively regulates Tkv in the P compartment by downregulating the mtv expression. Hh negatively modulates the *tkv* expression in cells of Hh signaling area by upregulating the mtv expression. Also, it was proposed that Dpp negatively regulate the *tkv* expression and thereby expands the spatial range of its own activity.[3,12,17]

Dpp binds to its receptor to form a Ligand-receptor complex which in turn phosphorylates Mother against Dpp to form pMad (See Figure 1). The level of pMad is usually considered as an indicator of Dpp signaling activity. The concentration of Dpp is not directly proportional to the level of Dpp signaling activity. In the wing disc, the pattern of pMad is very interesting[3] and can be seen in Figure 2 (A) and (B). In particular, in the P compartment, it is highest in cells near the AP boundary where the Dpp

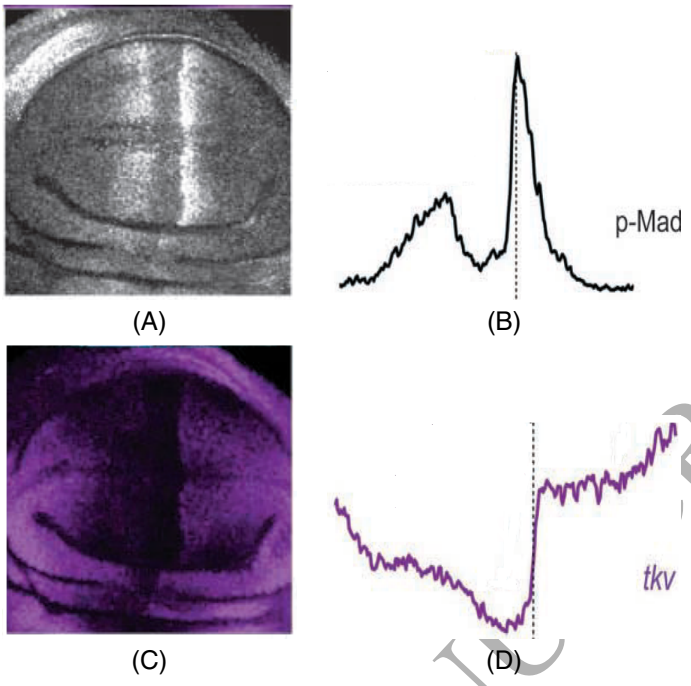

Figure 2: **(A),(B): Experimental measurement of pMad;[3] (C,D):Experimental measurement of *tkv* expression[3]**. For the image of wing disc in (A), the lightness reflects the intensity of pMad level which can be translated into curve of pMad concentration in (B). For the image of wing disc in (C), the intensity of pink color quantifies the level of *tkv* expression which can be described by the curve of *tkv* concentration.

concentration is high, and it decreases sharply in a short distance. In the A compartment, the level of pMad there is greatly reduced in cells adjacent to the AP boundary where both Hh and Dpp levels are high. It gradually becomes higher away from the AP boundary and forms a second steep gradient. The complex pattern of pMad is hypothetically contributed by the distribution of Tkv.[12] For instance, the dramatic reduction of pMad in the Hh signaling region can be due to the direct repression of Tkv by Hh in the area.[12]

Besides, there are many other discovered components in the Hh and Dpp signaling networks to probably play a specific role in the AP patterning, growth and scaling. For example, another BMP ligand Glass bottom boat (Gbb) may be required for the establishment of target gene expression domains over a long distance in both A and P compartments.[18] Gbb may preferentially interact with another type-I receptor Saxophone (Sax). Some experimental results suggest the dual function of Sax in the BMP signaling, i.e., when being together with Tkv it promotes the BMP signaling while alone it antagonizes the BMP signaling.[18] Moreover, previous studies proposed that Pentagone (pent) antagonizes the Dpp internalization and facilitates the Dpp transport through co-working with Glypicans Division abnormally delayed (Dally) and Dally-like (Dly) in Drosophila.[19] Furthermore, Dally/Dly may play an essential role in the Dpp transport as well as the Dpp signaling since the level of pMad is dramatically reduced in both Dally-Dly double mutant clones.[20] A summary of relatively complete understanding of complex signaling pathways and their interactions for patterning and growth in the wing disc can be found in a review paper by Umulis and Othmer.[4]

Therefore, development of the wing disc involves many interacting components as well as a variety of complex processes such as patterning formation, signaling transduction, gene expression, transport of molecular species, and growth. However, many underlying mechanisms of those processes remain a mystery or under investigation. In light of the complexity of interacting regulatory networks in the wing disc, rigorous mathematical models and analysis have to be applied for a better understanding of underlying mechanisms.[4] Computational modeling, coupled with quantitative measurements, has grad-

ually become a very useful tool for hypothesis test, data integration, and guidance for new experimental designs in the studies of developmental biology.[4] In fact, many previous attempts to quantitatively investigate the signaling activities in the developmental wing disc have been fruitful in term of discovering new exciting features and testing numerous hypotheses.[4,5,9] For instance, mathematical models were successfully proposed to examine the effects of dynamic pattern interpretation,[5,21] feedback-mediated regulation,[15] and coordination between growth and patterning.[22]

Regarding the Anterior-Posterior (AP) patterning in the wing disc, most of existing mathematical models and computational analysis focus on the P compartment partially due to the surprising complexity and asymmetry of patterning, such as the patterns of Tkv and pMad, throughout the whole disc.[9,11] Moreover, even if Dpp is one of the most extensively studied morphogens, it remains unclear about the underlying mechanisms for the gradient formation of Dpp signaling activity, Dpp scaling properties, and its role on growth control.[1,4,11] One of our objectives in this work is to develop a baseline mathematical model to investigate core mechanisms of the AP patterning of Drosophila wing discs. In particular, we focus on two major morphogens Hh and Dpp and their signaling activities. To the author's best knowledge, this is the first time that a mathematical model is used to study the morphogen Dpp signaling activity, which is indicated by pMad in this work and involves receptor Tkv, in both A and P compartments. To validate our proposed model, we test the computational spatial profiles of involved components against the experimentally-measured results. An important test is to determine whether the numerical distributions of *tkv* expression and pMad match the complex observed patterns near the AP boundary and whether we are able to regenerate the asymmetry of Tkv profile throughout the disc. In addition, specific roles of involved molecular components in the establishment of complex Tkv and pMad patterns are examined and some biological hypotheses are tested. By doing so, it may shed light on the underlying mechanisms of how the gradient of Dpp signaling activity is formed.

II Model and computational methods

Our mathematical model of the AP patterning consists of two modules. One is for the Hh signaling network which induces Dpp. The other one is Dpp signaling network. We attempted to derive a model of minimum players which is sufficient to reproduce complex experimental measurements of Tkv and pMad as displayed in Figure 2 (A)(B) and 2 (C)(D). To the end, we first assumed that a one-dimensional (1D) system could be used to describe the AP patterning of wing disc (See Figure 3). That is a reasonable approximation due to the facts that wing discs in Drosophila are approximately flat tissues[5,9] and that from all positions along the AP boundary Hh fluxes across the A compartment. Moreover, the AP boundary is assumed to divide the 1D domain into anterior (A) and posterior (P) compartments equally according to experimental images.[5]Furthermore, since the formation of morphogen gradient is much faster than cell proliferation[23], it is assumed that discs have a fixed size for our study term. By doing so, one decouples growth and patterning so that growth can be ignored as a first step.

Computationally, the total length of the AP axis is set to be 200 μm. The original point is regarded as the AP boundary which equally divides the whole domain into anterior ($[-100, 0)$) and posterior ($(0, 100]$) compartments (See Figure 3). This setup is based on at least two experimental measurements from the literature: One is that the AP axis of a third larval wing disc is about 80 cells long.[4,5,24] The other is that $2.5\mu m$ can be used as the average cell diameter on binding surfaces.[5,9,23]

II.A The mathematical model

Our proposed mathematical model was constructed based on a simple interaction network for the Hh and Dpp signaling shown in the lower panel of Figure 3. In our model, transport processes of mobile species are modeled with effective diffusion.[9] In addition, the mass-action law is used to describe ligand-receptor binding activities. Thus, the formation rate of a ligand-receptor complex is proportional to the product of ligand and receptor concentrations. As a result, the proposed model for the AP patterning in the wing disc is a system of Reaction-Diffusion (RDs) equations and Ordinary Differential Equations (ODES) in which mobile species are described by the RD equations, and immobile species are modeled with ODES.

Hh module

$$\frac{\partial [Hh]}{\partial t} = D_{hh}\frac{\partial^2 [Hh]}{\partial x^2} + (1 - a(x))\alpha_{enhh} - k^+_{hp}[Hh][Ptc] + k^-_{hp}[\overline{HP}] - \beta_{hh}[Hh] \quad (1)$$

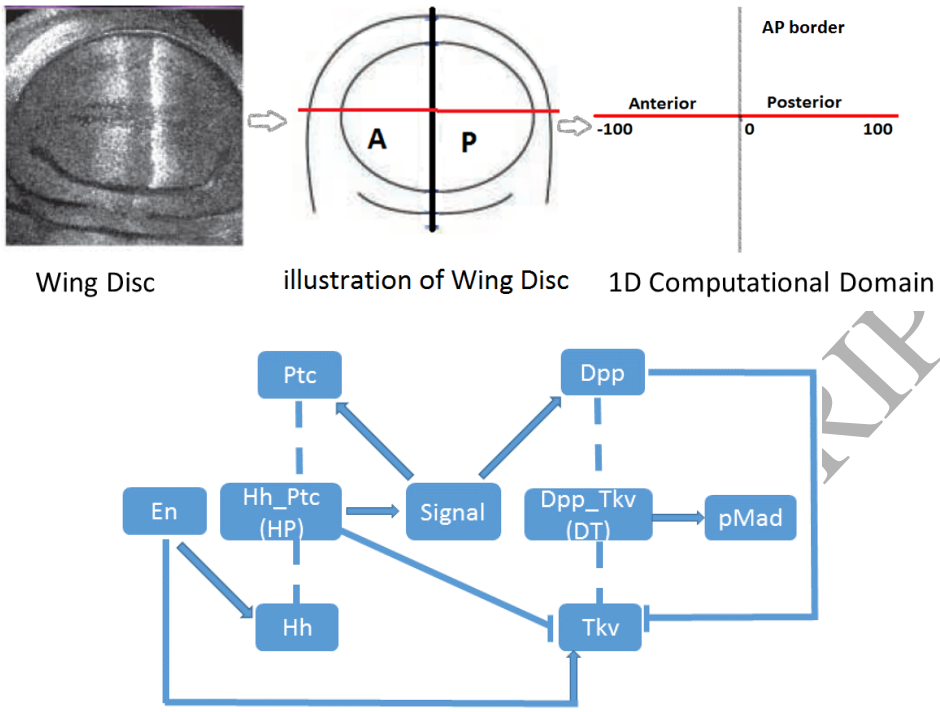

Figure 3: **upper panel: Simplified view of wing disc as a one-dimensional (1D) system; Lower panel: A proposed simple network for the Hh and Dpp signaling**. Because wing discs (left) in Drosophila are approximately flat tissues, it is reasonable to consider them as a two-dimensional (2D) system (middle). Moreover, from all positions along the AP boundary, Hh fluxes across the A compartment and Dpp transports in both A and P compartments. Therefore, the 2D system can be further simplified into a one-dimensional (1D) system (right). In our 1D computational domain, the AP boundary is considered to divide the whole computational domain equally into anterior and posterior compartments. The left two figures of upper panel are taken from Tabata et al.[3] with some revisions. For the network flow of lower panel, dotted lines represents binding of ligand and receptor to form a complex. For example, Dpp and Tkv bind to form Dpp-Tkv complex. Arrow-headed lines and bar-headed lines are used to indicate activation (or upregulation) and inhibition (downregulation), respectively. All involved interactions are supported by some existing accepted experimental observations: Engrailed (En) induces the Hh expression in the P compartment: Ligand Hh and its receptor Ptc form Hh-Ptc complex to activate the Hh signaling;[5] Hh signaling induces the gene *dpp* expression and gene *ptc* expression near the AP boundary in the A compartment;[3] Tkv is a preferred receptor of Dpp in the wing disc[12,16] and its level is probably downregulated by Dpp;[16] Hh signaling is found to repress Tkv levels near the AP boundary and the level of Tkv in the P compartment is upregulated by En.[16] Dpp binds Tkv to phosphorelate Mothers Against Dpp (pMad).

$$\frac{\partial[Ptc]}{\partial t} = a(x)\alpha_{Ptc} + \alpha_{sigptc}\frac{[Signal]^p}{(M_{Ptc})^p + [Signal]^p} - k_{hp}^{+}[Hh][Ptc] + k_{hp}^{-}[\overline{HP}] - \beta_{Ptc}[Ptc] \tag{2}$$

$$\frac{\partial[\overline{HP}]}{\partial t} = -k_{hp}^{-}[\overline{HP}] + k_{hp}^{+}[Hh][Ptc] - \beta_{hp}[\overline{HP}] \tag{3}$$

$$\frac{\partial[Signal]}{\partial t} = \alpha_{signal}\frac{(\frac{[\overline{HP}]}{[Ptc]})^s}{(M_{signal})^s + (\frac{[\overline{HP}]}{[Ptc]})^s} - \beta_{signal}[Signal] \tag{4}$$

where $[Hh], [Ptc]$ and $[\overline{HP}]$ are concentrations of Hh, Ptc, and the Hh-Ptc complex, respectively. The variable [Signal] is introduced for the concentration of Hh signaling activity so that the intensity to activate the Hh target gene expressions is simply reflected by the level of [Signal]. Here there is not a particular molecular mechanism about how the Hh-Ptc complex and Ptc produce intracellular signaling activity. Regarding the parameter notations, D_{hh} is the diffusion coefficient for Hh; k_{hp}^{+} represents the association

rate of the Hh-Ptc complex; k_{hp}^{-} is taken as corresponding dissociation coefficient. $\beta_{(\cdot)}$ is used for rates of degradation. a(x) is a characteristic function of the A compartment in which $a(x) = 1$ in the A compartment and $a(x) = 0$ in the P compartment.

In our model, constant rates are taken to describe ubiquitous activation or induction, while Hill functions are used for activation or regulation with a threshold. Specifically, α_{enhh} is for the ubiquitous activation rate of Hh by Engrailed in the P compartment, and α_{Ptc} is for the ubiquitous expression rate of Ptc throughout the wing disc. In addition, the positive feedback of Hh signaling on Ptc is modeled by a Hill function $\alpha_{sigptc}\frac{[Signal]^p}{(M_{ptc})^p+[Signal]^p}$ where α_{sigptc} is the maximum upregulation rate and M_{ptc} is the level of [Signal] at which the upregulation rate of Ptc reaches half of its maximum level. The activation rate of Hh signaling is described by another Hill function $\alpha_{signal}\frac{(\frac{[\overline{HP}]}{[Ptc]})^s}{(M_{signal})^s+(\frac{[\overline{HP}]}{[Ptc]})^s}$ in which α_{signal} is the maximum activation rate and M_{signal} is the value of ratio $\frac{[\overline{HP}]}{[Ptc]}$ at which the activation rate of Hh signaling [Signal] reaches half of its maximum value. Both s and p are constant parameters. Here we adopted experimental observations that Hh signaling activity depends on the ratio of Hh-Ptc complex and Ptc concentrations.[5]

Remark that current Hh module was modified from a previous model of Hh signaling by Nahmad et al.[5] In order to obtain a mathematical model which is capable of reproducing complex Tkv and pMad profiles with as few network components as possible, we did not consider gene *ptc* in our model. Because of it, the production and upregulation of gene *ptc* by the Hh signaling need to be directly considered in the equation of the Hh receptor ligand Ptc. As a result, we proposed a new equation for Ptc in Equation (2). Meanwhile, our Hh module has one less equation than the Nahmad's.

Dpp module

$$\frac{\partial[Dpp]}{\partial t} = D_{dpp}\frac{\partial^2[Dpp]}{\partial x^2} + \alpha_{sigdpp}\frac{[Signal]^d}{(M_{dpp})^d+[Signal]^d} - k_{dt}^{+}[Dpp][Tkv] + k_{dt}^{-}[\overline{DT}] \tag{5}$$

$$\frac{\partial[Tkv]}{\partial t} = \alpha_{tkv}+(1-a(x))\alpha_{entkv}-\frac{r_{dpptkv}[Dpp]}{[Dpp]_{max}}-\frac{r_{hhtkv}(\frac{[\overline{HP}]}{[Ptc]})^n}{(M_{tkv})^n+(\frac{[\overline{HP}]}{[Ptc]})^n}-k_{dt}^{+}[Dpp][Tkv]+k_{dt}^{-}[\overline{DT}]-\beta_{tkv}[Tkv] \tag{6}$$

$$\frac{\partial[\overline{DT}]}{\partial t} = k_{dt}^{+}[Dpp][Tkv] - k_{dt}^{-}[\overline{DT}] - \beta_{dt}[\overline{DT}] \tag{7}$$

where $[Dpp], [Tkv]$ and $[\overline{DT}]$ are concentrations of Dpp, free Tkv protein and the Dpp-Tkv complex, respectively. D_{dpp} is the effective diffusion coefficient of Dpp; k_{dt}^{+} represents the association coefficient of the Dpp-Tkv complex; k_{dt}^{-} is for the dissociation coefficient.

In the Dpp module, the Dpp degradation in the wing disc is described in the formula of Dpp-Tkv complex $\overline{DT}$ in Equation (7) instead of Equation (5) for Dpp, since it turned out that the degradation is most likely receptor driven.[25,26] In the same spirit as that in the Hh module, a constant rate is for ubiquitous activation or induction, and Hill functions for activation or regulation with a threshold. In particular, α_{tkv} is used as the ubiquitous activation rate of Tkv . α_{en} denotes the induction rate of Tkv by the transcription factor En in the P compartment.[3,16] Moreover, $\alpha_{sigdpp}\frac{[Signal]^d}{(M_{dpp})^d+[Signal]^d}$ describes the induction rate of Dpp by the Hh signaling. And the downregulation rate of Tkv by the Hh signaling is taken into consideration by subtracting a Hill function $\frac{r_{hhtkv}(\frac{[\overline{HP}]}{[Ptc]})^n}{(M_{tkv})^n+(\frac{[\overline{HP}]}{[Ptc]})^n}$[3,16] in which it is assumed that the repression also depends on the ratio of Hh-Ptc complex and Ptc concentrations.[6] Finally, to explore the potential downregulation of Tkv by Dpp,[4,12] we adopted a linear function of $[Dpp]$ formulated as $\frac{r_{dpptkv}[Dpp]}{[Dpp]_{max}}$, where r_{dpptkv} is the maximum repression rate and $[Dpp]_{max}$ is the maximum Dpp concentration to normalize the Dpp intensity in our computation. Actually, a Hill function can also be used to model the repression

of Tkv by Dpp to regenerate similar profiles (data is not shown here). Note that in Equation (6) we used the term $\frac{r_{dpptkv}[Dpp]}{[Dpp]_{max}}$ to reflect a direct regulation by a Dpp-receptor complex (rather than Dpp-tkv) whose concentration is proportional to free Dpp concentration. For instance, Dpp may negatively modulate the *tkv* expression via binding with another type-I receptor Sax, which is uniformly distributed in the wing disc,[18] to form Dpp-Sax complex. It can be shown that $[Dpp - Sax]$ is linearly proportional to $[Dpp]$ at equilibrium state due to constant [Sax]. In addition, in Equation (6), we imposed a parameter constraint $\alpha_{tkv} - r_{dpptkv}\frac{[Dpp]_{nummax}}{Dpp_{max}} - r_{hhtkv} > 0$ in order to guarantee that the net activation rate of Tkv is always biologically non-negative even in the presence of repressions. Here $[Dpp]_{nummax}$ represents a pre-estimated numerical maximum of [Dpp] level from our simulation without the Dpp-dependent repression term.

II.B Parameter estimate

The present model contains more than 20 parameters such as effective diffusion coefficients, binding parameters, and degradation rates. It is well known that biologically plausible parameter values play an essential role for a meaningful and powerful mathematical model. Although those involved parameters are not precisely known, their reasonable range can be estimated according to in vitro experimental measurements, biacore binding data, and other existing related resources. A base set of parameter values used in our simulations is listed in Table 1 and Table 2 for the Hh module and Dpp signaling module, respectively. In the Appendix, supporting literature and evaluating processes are given in details for chosen parameter values in our model simulations. Moreover, parameter sensitivity analysis, which will be described in section III.C, can demonstrate the robustness of our model against parameter changes within a certain range.

Table 1: Parameter values for the Hh module.

Symbol	Description	Value	Reference
D_{hh}	Hh diffusion coefficient	0.5 $\mu m^2/s$	5,23
α_{hh}	Hh maximal activation rate	$3.4 \times 10^{-3} \mu M s^{-1}$	5
α_{Ptc}	Ptc maximal activation rate	$9.8 \times 10^{-5} \mu M s^{-1}$	This work
α_{sigptc}	Signal induction rate	$6.9 \times 10^{-4} \mu M s^{-1}$	This work
α_{signal}	Signal maximal activation rate	$1.6 \times 10^{-4} \mu M s^{-1}$	5
β_{hh}	Hh degration rate	$3.3 \times 10^{-3} s^{-1}$	5
β_{Ptc}	Ptc degration rate	$1.5 \times 10^{-3} s^{-1}$	5
β_{hp}	Hh-Ptc complex degration rate	$1.5 \times 10^{-3} s^{-1}$	5
β_{signal}	Signal degration rate	$5.5 \times 10^{-4} s^{-1}$	5
k_{hp}^{+}	Hh-Ptc associate rate	$7.15 \times 10^{-2} \mu M^{-1} s^{-1}$	5,9
k_{hp}^{-}	Hh-Ptc de-associate rate	0 s^{-1}	5
M_{Ptc}	Ptc half-maximal activation	0.14 μ M	This work
M_{signal}	Signal half-maximal activation	2.135	5
p	Hill coefficient (Ptc)	3	5
s	Hill coefficient (Signal)	6.8	5

II.C Other computational setting

For extracellular bindings and reactions, initial and boundary conditions are needed. In our model, initial conditions for all species or complexes are set to be zero before the onset of the system except for Ptc. This is supported by an experimental result that the wild-type patterning can be sufficiently rescued when one re-initializes the system artificially with [Hh]=0.[29] For the initial condition of Ptc, it is set as done previously:[5]

$$[Ptc](x,0) = \frac{a(x)\alpha_{Ptc}}{\beta_{Ptc}} \tag{8}$$

Moreover, zero-flux is taken as boundary conditions (B.C.) of mobile morphogens Hh and Dpp at

Table 2: Some parameter values for the Dpp signaling module.

Symbol	Description	Value	Reference
D_{dpp}	Dpp Diffusion	0.5 $\mu m^2/s$	23,25,27
β_{dt}	Dpp-Tkv complex degration rate	$2.52 \times 10^{-4} s^{-1}$	9,23,25
k_{dt}^{+}	Dpp-Tkv association rate	$0.1 \mu M^{-1} s^{-1}$	5,9
$[Dpp]_{max}$	maximum level of Dpp	0.9μ M	23
$[Tkv]_{max}$	maximum level of Tkv	0.34μ M	5,9[a]
α_{sigdpp}	dpp maximal activation rate	$2 \times 10^{-4} \mu M s^{-1}$	This work
α_{tkv}	Tkv production rate	$8.57 \times 10^{-5} \mu M s^{-1}$	This work
α_{en}	Engrail based production rate	$6.85 \times 10^{-5} \mu M s^{-1}$	This work
r_{hhtkv}	Hh maximal repression rate	$3.43 \times 10^{-5} \mu M s^{-1}$	This work
r_{dpptkv}	dpp maximal repression rate	$1.71 \times 10^{-4} \mu M s^{-1}$	This work
β_{tkv}	Tkv degration rate	$2.52 \times 10^{-4} s^{-1}$	This work
k_{dt}^{-}	Dpp-Tkv de-association rate	$0.0067 s^{-1}$	This work
M_{dpp}	Dpp half-maximal activation	0.05 μ M	28
M_{tkv}	Tkv half-maximal repression	2.135	5
d	Hill coefficient (Dpp)	3	5
n	Hill coefficient (Tkv)	6.8	5

[a] It is not experimental data but theoretical estimation as shown in the Appendix V.B

$x = \pm 100\ \mu m$. That is a good approximation because the range of both Hh and Dpp gradients is short compared to the size of each compartment. Our model system was numerically solved using a MATLAB code. Specifically, function ode15s was adopted for solving the system of differential equations. All of results shown in this paper were computed with 160 grid points.

III Computational results and discussions

III.A Validation

In this section, numerical spatial profiles of individual components generated by our proposed model of AP patterning are compared with experimental measurements from the literature. Completion of these comparisons can validate the model and build a solid base for further model development and analysis. In particular, it is shown that our model is able to accurately reproduce complex experimentally-measured patterns of *tkv* expression and pMad in both anterior and posterior regions of wing disc. Meanwhile, it is capable of generating observed overshoots of Hh gradients and its signaling activities.

III.A.1 Dpp signaling

An important test is to determine whether complex distributions of *tkv* expression and pMad can be reproduced around the AP boundary using the present model. pMad is normally used as a downstream marker to demonstrate the Dpp signaling activity.[3] In the Drosophila wing disc, the level of pMad is not directly proportional to the Dpp level (see Figure 2(A) and (B)) for wild-type pMad profile and Figure 6 for Dpp). Specifically, the pMad level is high in cells near the AP boundary in the P compartment , but is greatly reduced along the AP boundary in the A compartment where Dpp is expressed and the level of Dpp is very high. Regarding the profile of Dpp receptor Tkv (see Figure 2(C) and (D)), its concentration of the A compartment reaches lowest a few cell diameter away from the AP boundary and gets higher away from the Dpp secretion region. In contrast, the level of *tkv* expression sharply increases near the AP boundary in the P compartment. In addition, the *tkv* concentration is generally higher in the P compartment than it is in the A compartment.

It turns out that our proposed model is able to regenerate complex profiles of pMad and *tkv* expression throughout the whole computational domain. To display the pMad profile, for simplicity the level of pMad is assumed to be linearly proportional to the level of Dpp-Tkv complex ($\overline{DT}$). This assumption is inspired by experimental observations that the absolute number of occupied receptors is linearly proportional to the level of nuclear Smad protein.[12,30] Consequently, it is not necessary for us to explicitly compute pMad in order to demonstrate the Dpp signaling activity. The 1D numerical profile of pMad throughout

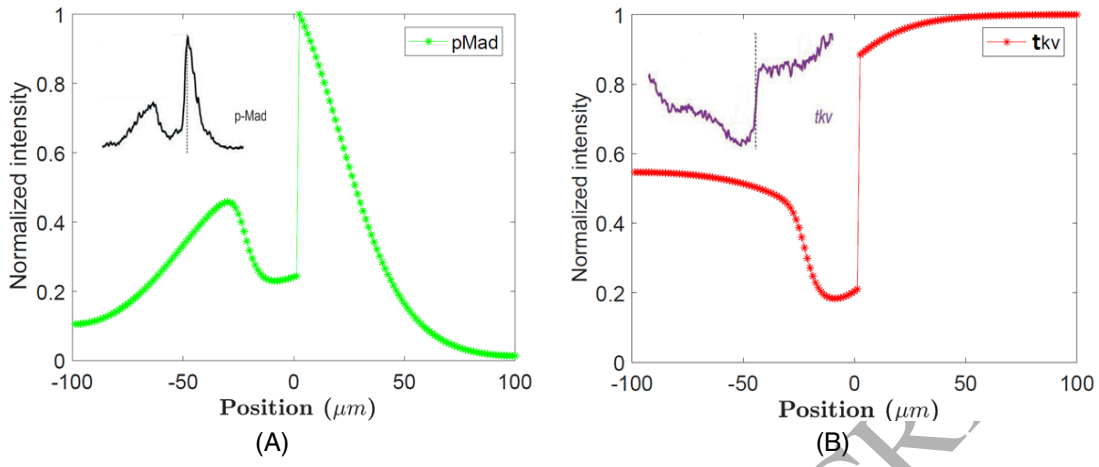

Figure 4: **(A): Numerical profile of pMad ; (B): Numerical profile of *tkv* expression**. Our numerical profile of pMad perfectly fits the experimental measurement (left corner one or see Figure 2: Firstly, the level of pMad is low in the Hh expression area despite of high level of Dpp. Secondly, there exist two concentration steep gradients. The lower peak is located away from the AP boundary and the higher peak occurs abutting to the AP boundary in the P compartment. Note that the normalized intensities of species in this and the following figures are obtained through dividing numerical concentration by the maximum computed concentration of corresponding species. Moreover, our numerical Tkv pattern matches the experimental observation very well except for the periphery regions where the *tkv* expression levels climb sharply: it displays the lowest Tkv expression in the Dpp expression region , and the level of *tkv* gets higher away from the AP boundary in both A and P compartments. Moreover, in general the level of *tkv* is higher in the P compartment than that in the A compartment. Actually, mechanisms of the sharp increase of Tkv level in the periphery regions are not clearly disclosed yet[16] and will be intensively pursued in our another work.[31]

the whole wing disc is displayed in Figure 4(A). It perfectly fits the experimental measurement in Figure 2 (B). Moreover, to show the level of *tkv* expression in this work, we used the concentration of total Tkv protein which consists of free Tkv proteins ([Tkv]) and bound Tkv proteins ($[\overline{DT}]$) since it can been shown that the concentration of gene *tkv* expression is proportional to the level of total Tkv protein at the equilibrium state (See details in the Appendix V.A). The *tkv* expression profile in Figure 4(B) matches the experimental observation very well except for the periphery regions where the *tkv* levels climb sharply. Actually, mechanisms of the sharp increase of *tkv* level in the periphery regions are not clearly disclosed yet[16] and will be pursued in our on-going work.[31] Here all normalized intensities of species in the figures of the present work are obtained through dividing their numerical concentration by the maximum concentration of corresponding species.

Quantitatively, our numerical results also agree with existing experimental data. For instance, it was experimentally measured that Dpp is activated in 7-8 cells starting from the AP boundary in the A compartment of wing disc.[32] Our numerical Hh signaling length is about 20 μm which is equal to 7-8 cell diameters (the average diameter of one cell is $2.5\mu m$ in current setting). Moreover, with our basic set of parameters, the numerical decay length of Dpp (see Figure 6) is $21.25\mu m$ which is exactly located at the measured set of decay length of Dpp $20.2 \pm 5.7\mu m$.[23] Here the decay length of a species is calculated with the distance from the AP boundary to the position where its concentration decays in the P compartment by a factor $\frac{1}{e}$ in comparison with the concentration level at the AP boundary . Furthermore, using our model, one is able to quantitatively predict certain individual patterning features which may not be reported in the literature. For instance, the position of the second maximum peak of pMad concentration which is located in the A compartment, as well as the pMad decay length, can be computed easily by current model. With our basic parameter set, the predicted decay length of pMad is 36.25 μm which is comparable to semi-experimental data.[33] In addition, the predicted second maximum peak of pMad in the A compartment is 30.00 μm away from the AP boundary.

The ability of the present baseline model in reproducing complex profiles of Tkv and pMad is most likely thanks to that we have incorporated into our model several important experimental observations and corresponding hypothesized mechanisms. These observations have been described in Introduction

Table 3: Quantitative comparisons between numerical results and experiment.

Quatity	Numerical	Experiment
Activation length of dpp	7-8 cells	7-8 cells[32]
Dpp decay length in the P compartment	21.25 μm	$20.2 \pm 5.7 \mu m$[23]
pMad decay length in the P compartment	36.25 μm	$25.2 \pm 4.5 \mu m$[33]
Second maximum peak of pMad	30.00 μm	N/A

and Modeling sections and now summarized as follows: First of all, on the one hand, the Dpp signaling activity, which is represented by pMad here, may be regulated by the distribution of Tkv that is considered as the preferred type I receptor of Dpp in the wing disc.[3,12,16] On the other hand, the level of Tkv may be downregulated by the Dpp signaling[16] and this hypothesis is considered by term $r_{dpptkv}[Dpp]/[Dpp]_{max}$ in Equation (6). Secondly, the level of Tkv is also dynamically regulated by En and Hh through master of thickveins (mtv) which downregulates *tkv* expression.[3] In particular, Hh represses Tkv levels and this is modeled with term $a(x)\frac{r_{hhtkv}(\frac{[HP]}{[Ptc]})^n}{(M_{tkv})^n+(\frac{[HP]}{[Ptc]})^n}$ in Equation (6). Moreover, high level of Tkv in the P compartment is positively regulated by En,[16] and the mechanism is taken into consideration by term $(1-a(x))\alpha_{en}$ in Equation (6). As a result, the dramatic reduction in the pMad concentration along the AP boundary in the A compartment can be a direct result of duo repressive actions of Hh and Dpp on Tkv. Moreover, higher Tkv expression in the P compartment than it is in the A compartment can be contributed by En. However, it remains unclear on how Hh, Dpp and En corporate to produce the observed complicated spatial patterns of Tkv and pMad. The specific roles of individual components on the Tkv and pMad patterning are examined in the section (III.B).

III.A.2 Another validation by Tkv mutation and Dpp overexpression

It is interesting to see that our model can also reproduce mutant or overexpression phenotypes without any change of parameters. First of all, we tested whether eliminating *tkv* function leads to the absence of pMad as observed.[12] To the end, we set $[Tkv] = 0\mu M$ which really leads to no pMad. Moreover, our model is able to reproduce the dramatic changes of *tkv* expression and pMad profiles in discs that ubiquitously express dpp.[12] To mimic the overexpression of Dpp, we set the Dpp level as a constant throughout the whole domain by making $[Dpp] = 0.2\mu M$. It turned out that our numerical predictions perfectly matches experimental phenotypes and captures all the dramatic changes due to excess Dpp. The comparisons can be found in Figure 5. In particular, the distribution of pMad was ubiquitously elevated except at the AP boundary; Also, the level of pMad at the AP boundary was unchanged in the presence of Dpp overexpression; In addition, The pMad level was higher in the P compartment than that in the A compartment. For the pattern of *tkv* expression: frstly, the level of peripheral *tkv* was significantly reduced to the basal level; secondly, the basal level of *tkv* in the P compartment was still higher than in the A compartment; thirdly, the *tkv* level at the AP boundary remained hyperrepressed.

III.A.3 Overshoot of Hh and its signaling

Spatial 'overshoot' is a transient expansion of a morphogen gradient before it approaches its final steady-state distribution. The existence of overshoot behaviors of Hh and its downstream signaling was supported by in vivo evidence.[5] Aided by a computational model, Nahmad et al. proposed that the overshoot of the Hh gradient plays an instructional role for the Hh-dependent patterning and target gene expression in the Drosophila wing disc. Ptc up-regulation by Hh causes a transient expansion of the Hh gradient before it reaches the final distribution, which is required to distinguish different spatial domains of Hh target gene expression. Interested readers can find the details of Hh overshoot discussions in their paper.[5]

Current Hh signaling module was modified from the model proposed by Nahmad et al.[5] It is interesting to see whether our modified Hh module itself can reproduce the overshoot behavior of Hh gradient dynamics. To this end, profiles of Hh and its signaling activity, represented by [Signal], were plotted at two time points (transient time and steady state time). It turns out that the steady-state of Hh and its signaling can be achieved at $t_{ss} = 300$ minutes. We set the transient time at $t_{ts} = \frac{2}{3}t_{ss}$ minutes. Then the overshoots of Hh and its signaling can be clearly observed from our numerical results in Figure 6

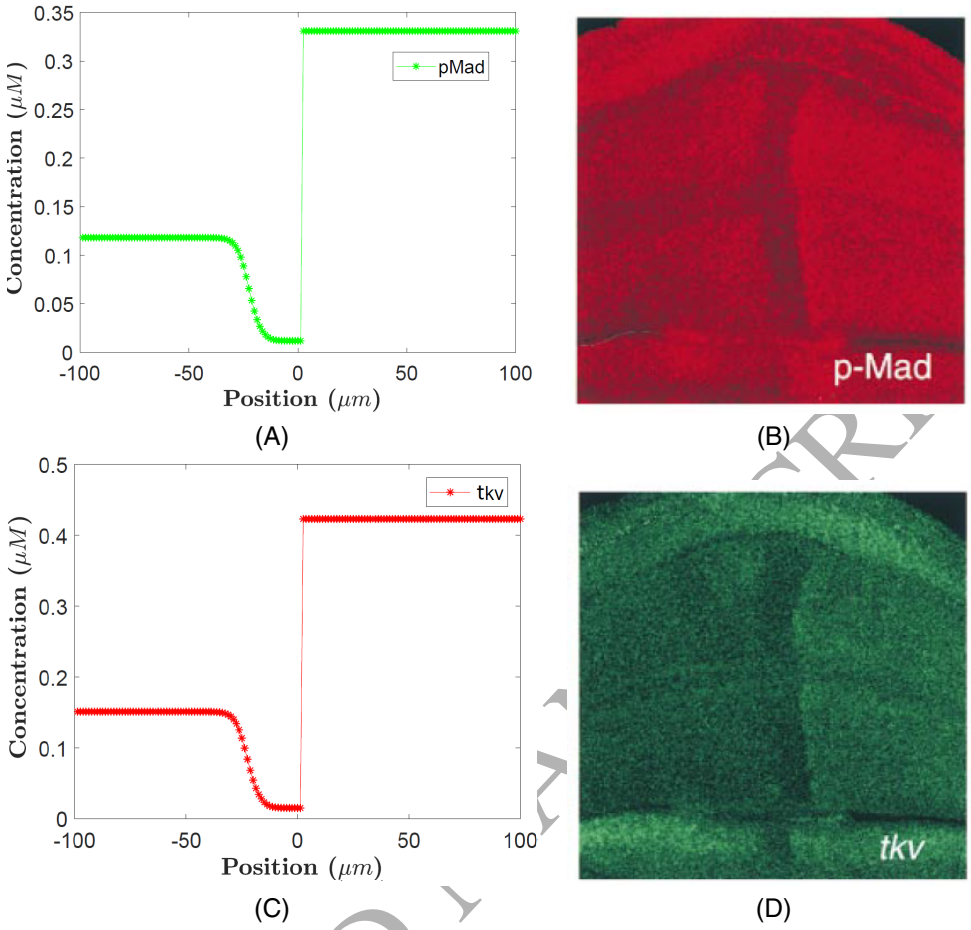

Figure 5: **Computational patterns of *tkv* expression and pMad match the experimental observations in the presence of excess dpp expression**. (A)numerical profile of resulting pMad; (B) Experimental image of pMad measurement in the disc where the lightness of red color reflects the magnitude of pMad level. It shows that our numerical predictions are consistent with the experimental outcomes and captures all dramatic changes due to excess dpp. (C) Computational profile of *tkv* expression; (D) Experimental image of *tkv* expression in the disc that ubiquitously express dpp in which the lightness of green color reflects the intensity of *tkv* expression level. Note that (B) and (D) are taken from Figure 5 (B) of paper[12] by Tanimoto et al.

(A)(B) where green lines represent the numerical solutions at transient time t_{ts} and blue lines for the steady-state solutions. Note that in Figure 6(A)(B), only part of the A compartment is shown. In addition, the complete Hh profile is displayed in Figure 6 (C), as well as its signaling activity indicator [Signal] and induced Dpp whose profile is shown in Figure 6(D).

III.B Specific roles of individual components on the Tkv and pMad patterning

In this section, we apply our validated model to explore specific individual roles played by Hh, Dpp, and En in the establishment of complex profiles of Dpp receptor Tkv and Dpp signaling activity that is indicated by pMad. By doing so, it may help us to understand the underlying mechanisms of existing experimental results better, provide a digital platform for testing existing hypotheses, and to inform potential new features of the AP patterning in the Drosophila wing disc. Our testing factors include (i) upregulation of Tkv by En in the P compartment, (ii) Hh repressing Tkv expression in Hh signaling cells, and (iii) downregulating Tkv by Dpp. All these analyses will be carried out by manipulating corresponding terms in the model and then comparing results between different situations.

It turns out that all En, Hh, and Dpp play an essential role in establishing complex experimentally-observed profiles of pMad and *tkv* expression in the whole wing disc. First of all, upregulation of the

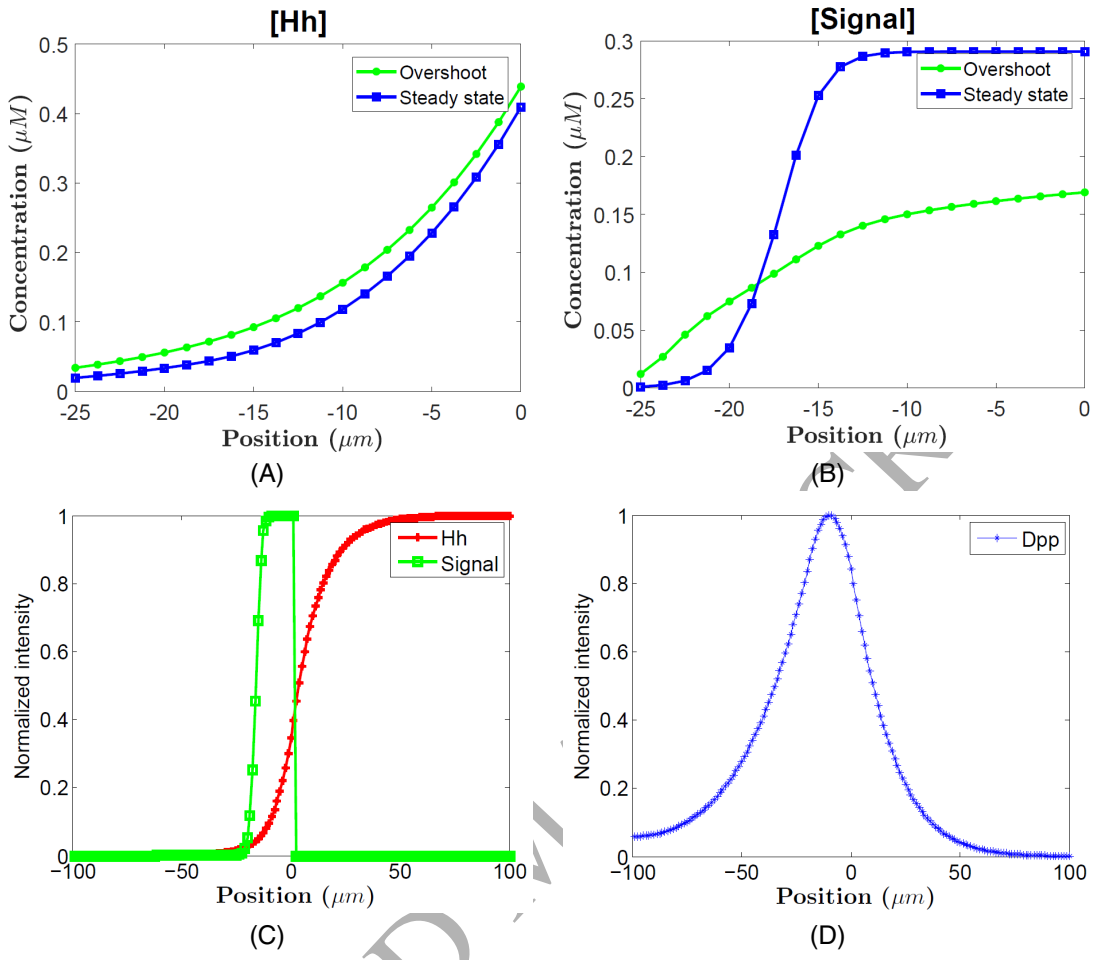

Figure 6: **(A) numerical overshoot of Hh gradient ; (B) computational overshoot of Hh signaling indicated by [Signal]; (C) Complete Profiles of Hh and its signaling indicated by [Signal] at a steady state in the whole wing disc domain (D) The complete profile of Dpp at a steady state.** Spatial 'overshoot' is a transient state in which the morphogen profile is expanded before approaching its final steady state,[5] and it has been postulated to play an instructional role for the Hh-dependent patterning and target gene expression in the Drosophila wing disc. In subfigures (A) and (B), the steady state solutions (represented by blue lines) are obtained at $t_{ss} = 300$ minutes, and the overshoots of transient time are plotted with solutions at $t_{ts} = \frac{2}{3}t_{ss} = 200$ minutes. Note that in numerical results of subfigures (A)(B), the origin is used to represent the AP boundary and the A compartment is on its left-hand side.

Tkv level by En determines the sharp jump of pMad across the AP boundary and the highest peak of pMad in the cells abutting to the AP boundary. It also helps to generate both steeper gradient of pMad and shorter effective range of Dpp in the P compartment than those in the A compartment. Secondly, short-range morphogen Hh downregulates the Dpp signaling activity through the repression of Tkv in the same cells in which Hh induces the Dpp expression. The Tkv suppression by Hh may simultaneously prevent the Dpp signaling from interfering and expands the effective range of Dpp gradient. Thirdly, Dpp negatively modulates Tkv to result in a gradual increase of Tkv distribution toward the peripheries of both A and P compartments. By doing so, Dpp facilitates itself spreading and shape the detailed local profiles of Tkv and pMad gradients. Meanwhile, the presence of Dpp repression of Tkv locates the local minimums of pMad and Tkv a few cell diameters away from the AP boundary, as shown from the experimental measurement.

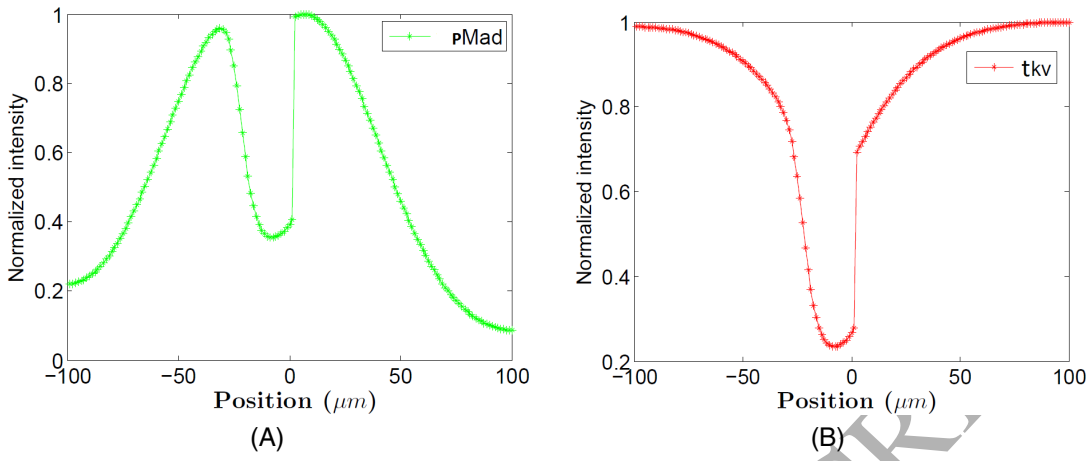

Figure 7: **The role of Engrailed (En) in the establishment of pMad (A) and *tkv* expression (B) profiles:** (A): The numerical pattern of pMad without the Engrailed (En) upregulation on Tkv by setting $r_{en} = 0$; (B): The computational profile of *tkv* expression in the absence of the upregulation of Tkv by En. Different from experimental observations,[3] in the absence of the En promotion of Tkv, there is no apparently sharp jump of pMad level in cells across the AP boundary in (A). Moreover, one can not see a higher level of *tkv* expression in the P compartment than in the A compartment in (B).

III.B.1 Upregulation of Tkv by En in the P compartment

To demonstrate the effect of En in generating the complex profiles of pMad and Tkv,[16] we simply turned off the En upregulation term in Equation (6) by setting $\alpha_{en} = 0$. It turns out that in the absence of En upregulation, there is no obviously sharp jump of pMad level in cells across the AP boundary. This is displayed in Figure 7 (A). Moreover, without the upregulation of Tkv by En, one can not see a higher level of Tkv expression in the P compartment than in the A compartment (See Figure 7 (B)). Therefore, it indicates that the promotion of Tkv by En determines not only the higher level of Tkv in the P compartment but also the sharp jump of pMad level across the AP boundary. As a result, the higher level of Tkv in the P compartment can account for the steeper gradient of pMad in the P compartment than it is in the A compartment since Tkv can trap Dpp via binding.

III.B.2 Hh repressing Tkv in Hh signaling cells

It has been well studied that Hh signaling induces the expression of gene *dpp*. To show another role of Hh in the Dpp signaling through the regulation of Tkv spatial distribution,[16] we first turned off the repression action of Hh signaling in Equation (6) by setting $r_{hhtkv} = 0 \mu M s^{-1}$. It is seen in Figure 8 (A) that without the repression of Tkv from Hh, the second peak of pMad disappears although the pattern of gene*tkv* expression matches the experimental observation (see Figure 8 (B)).

Moreover, to check whether more Dpp downregulation can substitute the impact of Hh downregulation, we enlarged the repression effects from Dpp by setting $r_{dpptkv} = 0.008 \mu M s^{-1}$ and $r_{hhtkv} = 0 \mu M s^{-1}$ to see whether the experimentally-observed patterns of *tkv* expression and pMad can be reproduced in the absence of Hh repression. It turns out that a rough pattern of pMad comparable to the experiment can be obtained (see Figure 8 (C)). However, the level of pMad is not severely reduced in cells of Hh signaling or Dpp expression region. This is contradictory to many experimental observations.[3,12,16] Therefore, our numerical model confirms the necessary dual roles of Hh on the Dpp signaling: Hh simultaneously induces the Dpp expression by binding with Ptc and lowers the Dpp signaling in the same cells of Hh signaling region through the downregulation of Tkv.[12]

III.B.3 Downregulating Tkv by Dpp

Previously, our model has demonstrated the individual roles of En and Hh in the formation of the pMad profile through the regulation of Tkv levels. The necessity of En and Hh participation was found in biological experiments.[3,12] And their underlying mechanisms have been extensively studied and most likely to involve Mtv.[16] In contrast, although negative modulation of Tkv by Dpp was proposed,[3,17] its existence and underlying mechanism remain unclear.

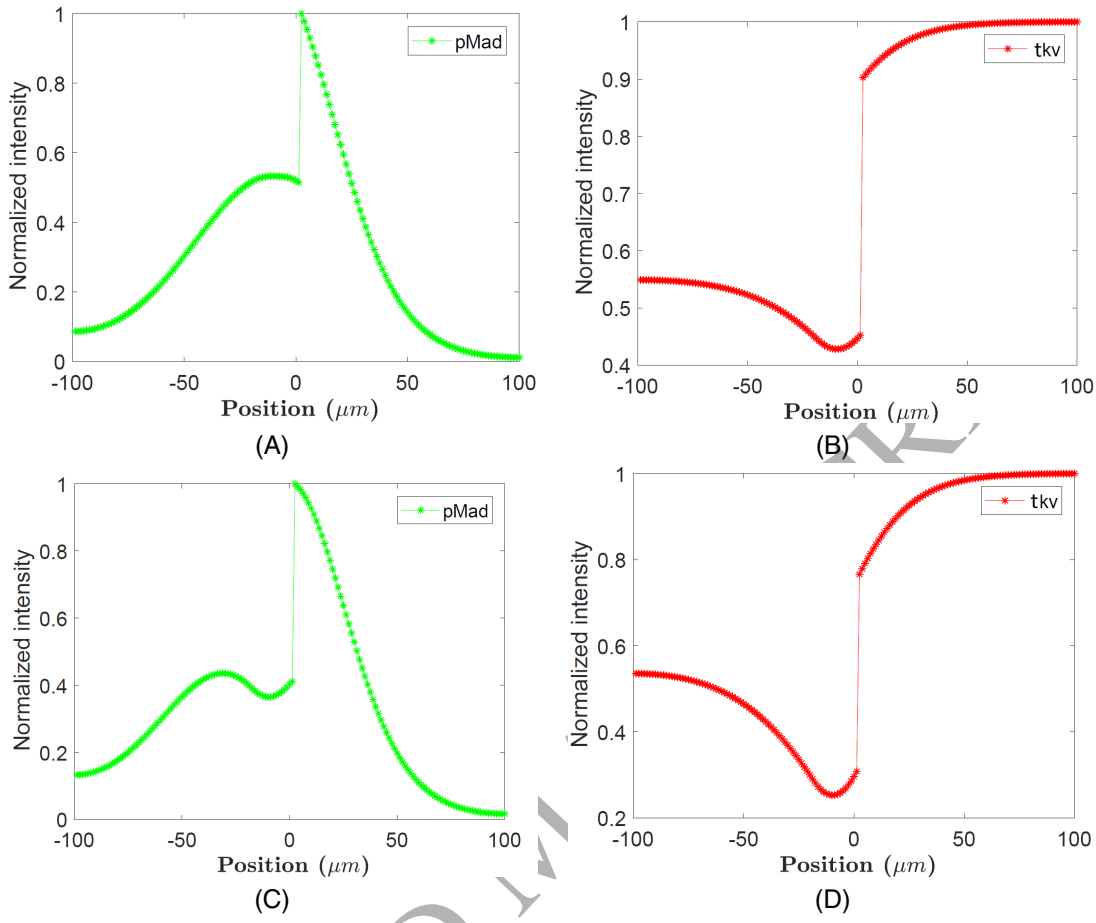

Figure 8: **The role of Hh in the establishment of *tkv* expression and pMad profiles.** First row: Computational profiles of pMad (A) and *tkv* expression (B) in the absence of downregulation of Tkv by Hh via setting $r_{hhtkv} = 0$. Second row: Numerical profiles of pMad (C) and *tkv* expression (D) without the downregulation of Tkv by Hh but with an enhanced downregulation of Tkv by Dpp via setting $r_{hhtkv} = 0$ and $r_{dpptkv} = 3.42 \times 10^{-4} \mu M s^{-1}$. Different from experimental observations,[3] the level of pMad is not severely reduced in cells of Hh signaling or Dpp expression region in (A) and (C) without the Hh repression.

Now it is interesting to see if the downregulation of Tkv by Dpp is indispensable, or whether the upregulation of Tkv by En and the downregulation of Tkv by Hh are sufficient to regenerate the patterns of *tkv* expression and pMad well. To this end, we turned off the repression term of Dpp by setting $r_{dpptkv} = 0 \mu M$. From the simulation results, one may observe at least a couple of obvious discrepancies between numerical results and their experimental counterparts. One is the position of local minimum points of *tkv* and pMad concentrations in the middle region of wing disc. Without the Dpp repression, the global minimum of *tkv* expression and local minimum of pMad level in the central area locate exactly at the AP boundary, while experimental measurements show that both of them are a few cell diameter away from the AP boundary.[3] This discrepancy can be observed by comparing Figure 2 (B) and Figure 9 (A) for pMad. The other discrepancy is the growing pattern of *tkv* levels toward the peripheries of both A and P compartments. In the absence of the Dpp repression of Tkv, there is no apparent gradual increase of *tkv* expression in the A compartment, and there is no change of *tkv* expression at all in the P compartment (See Figure 9 (B)). However, the gradual increase of *tkv* expression was observed in both A and P compartments[3] based on the experimental measurement in Figure 2 (D) and others. Even one enhances the repression rate of Hh by setting $r_{hhtkv} = 0.0016 \mu M s^{-1}$, and $r_{dpptkv} = 0 \mu M$, those discrepancies remain: These can be seen in Figure 9 (C)(D). Therefore, it has been demonstrated that

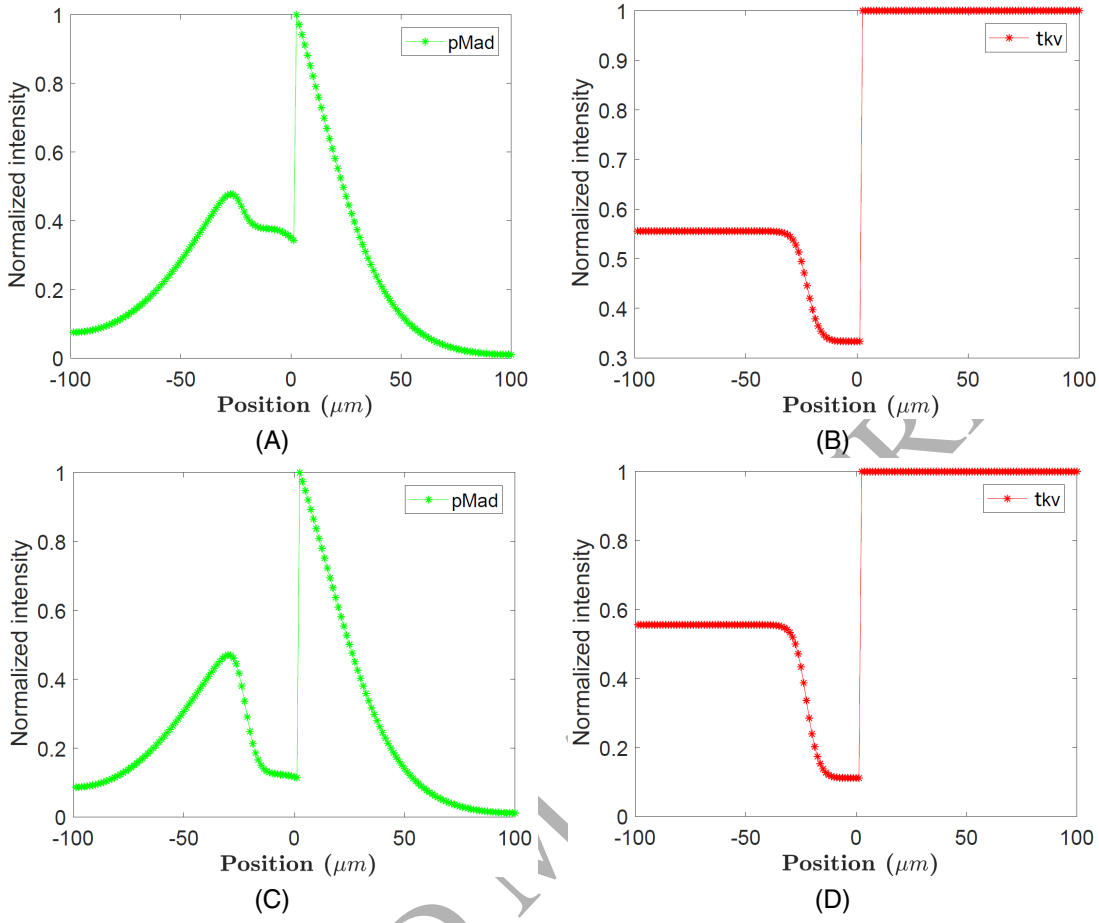

Figure 9: **The role of Dpp in the establishment of Tkv and pMad profiles.** First row: Numerical profiles of pMad (A) and *tkv* expression (B) in the absence of downregulation of Tkv by Dpp via setting $r_{dpptkv} = 0$. Second row: Numerical profiles of pMad (C) and *tkv* expression (D) without the downregulation of Tkv by Dpp but with an enhanced downregulation of Tkv by Hh via setting $r_{hhtkv} = 6.86 \times 10^{-5} \mu M s^{-1}$ and $r_{dpptkv} = 0$. Different from experimental observations,[3] the local minimums of both *tkv* expression and pMad locate exactly at the AP boundary in (A) and (C) in the absence of the Dpp repression of Tkv. Moreover, there is no obvious gradual increase of *tkv* expression in the A compartment, and there is no change of *tkv* expression at all in the P compartment in (B) and (D).

Dpp plays an essential role in shaping the detailed profiles of Tkv and pMad.

Moreover, our model may shed some light on the underlying mechanism of negative regulation of Tkv by Dpp. In this work, we tested whether Dpp signaling represses Tkv directly or not. First of all, it was found that the downregulation strength profile of *tkv* expression by Dpp can not be similar to the pattern of pMad level. Otherwise, it may result in several inconsistencies with the experimental observation. To see it, numerically we substituted $[Dpp]$ with $[DT]$ in the Dpp repression term of $\frac{r_{dpptkv}[Dpp]}{[Dpp]_{max}}$ in Equation (6). Consequently, local minimums of pMad and *tkv* in the central region of wing disc shift to the AP boundary, and there appears a much steeper change of *tkv* level from middle to the periphery of the P compartment than their experimentally-observed counterparts. Furthermore, there is no graded increase of *tkv* expression in the periphery regions of both A and P compartments. Those inconsistencies can be found in Figure 10.

Our explanation is given as follows: based on the experimental measurement, pMad is very high in cells adjacent to the AP boundary and decreases sharply in a short distance in the P compartment, and in the A compartment it has a low level at the place a few cell diameter away from the AP boundary. If

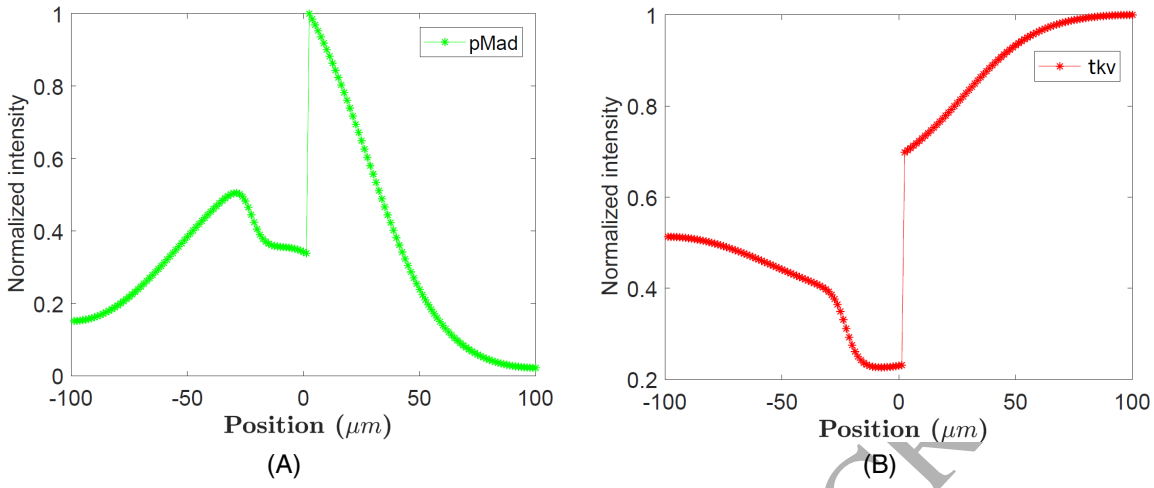

Figure 10: **The profiles of pMad and *tkv* expression if the repression strength profile of Tkv by Dpp similar to the pattern of pMad level is used**. It can be done through replacing $[Dpp]$ with $[DT]$ in the Dpp repression term of Equation (6). As a result of the substitution, the local minimums of pMad and *tkv* in the middle region of wing disc shift to the AP boundary, and there appears a much steeper change of *tkv* level from the middle to the periphery in the P compartment than experimentally observed counterparts.

the repression strength profile caused by Dpp has the same pattern as pMad, the repression strength will reach its local minimum at the position of the local minimum of the pMad level. Also, it generates a sharp change of Tkv levels near the AP boundary in the P compartment due to the significant change of pMad there. As a result, it would not be able to produce the observed pattern of *tkv* expression in which the most significant repression lies a few cell diameter away from the AP boundary, and there is no sharp change of Tkv levels from the AP boundary toward the periphery of the P compartment.

Indeed, a repression strength profile similar to the pattern of Dpp concentration (See Figure 6) turned out to be a relatively better candidate for the desired patterns of Tkv profile. To show that, we made the Dpp repression strength on Tkv in Equation (6) linearly proportional to the Dpp concentration rather than the level of Dpp-Tkv complex. Consequently, a good agreement reaches between simulations and the experiment for the patterning of Tkv and pMad. Our computational results of pMad and *tkv* expression capture major features of experimental measurements except that there are still no sharp climb of *tkv* expression in the periphery regions as observed experimentally. Therefore, our model suggests that Dpp signaling unlikely represses Tkv directly, and Dpp-dependent repression of Tkv may be in an indirect manner through Dpp downstream transcription factor, target genes and/or involving other components such as Dally. A detailed mechanism of negatively modulating Tkv by Dpp signaling will be intensively investigated in our another work.[31]

III.C Parameter sensitivity and robustness

As described in section II of Model and Computational methods, we selected some key parameters to form a base core set which includes diffusion coefficient, receptor/ligand binding parameters, and degradation. Then other parameters were estimated based on certain sound relationships with those core parameters. Those relationship formulas were derived according to some acceptable experimental measurements at steady state. For those parameters in the core set, the range of biologically plausible values may span over several-fold change or even several orders of magnitude in the literature. For instance, the diffusion coefficients of morphogen between $0.1\mu m^2 s^{-1}$ and $80\mu m^2 s^{-1}$ were used;[9,23] The range of degradation rate spans from $10^{-4}s^{-1}$ to $5\times10^{-3}s^{-1}$;[5,23,27] And the association rates varying from $0.01\mu M^{-1}s^{-1}$ to $16\mu M^{-1}s^{-1}$ were considered to be plausible.[9,34] Therefore, It is worthwhile to check whether the computational system is robust with respect to involved parameters, and to find out whether our results or conclusions are restricted to specific choices of parameter values.

In this section, the sensitivity of the computational system to specific choices of parameters is exam-

ined. We addressed the sensitivity of one single parameter each time and varied one single parameter with everything else held constant. To evaluate the sensitivity, we not only observed the qualitative similarity but also quantified the response of the system to the changes of a particular parameter.[35] Qualitatively we looked into the pattern features of pMad levels: 1. having extreme high concentration in cells abutting to the AP boundary and decreasing sharply in a short distance in the P compartment; 2. Being significantly reduced in cells adjacent to the AP boundary in the A compartment and then gradually becoming higher away from the AP boundary to form a second steep gradient; 3. the lowest level of the central region locates at a few cell diameters away from the AP boundary. Quantitatively, we calculated the decay lengths of both Dpp concentration and the level of pMad. Moreover, the position of the second peak of pMad level in the A compartment was tracked and recorded.

In particular, we evaluated the sensitivity of the Dpp Module to the changes of core parameters including $k_{dt}^{+}, D_{dpp}, \beta_{dt}$. To evaluate the sensitivity of our model system to the receptor/ligand binding rate, we varied k_{dt}^{+} over eightfold from $0.02\mu M^{-1}s^{-1}$to $3.2\mu M^{-1}s^{-1}$. It exhibits that the patterning of pMad is robust against the change of k_{dt}^{+}. With the value changing over eightfold, not only the pattern of the pMad level is maintained, but also the quantitative measurements of decay length of pMad and the position of its second peak. Results of the sensitivity of the Dpp module with respect to the changes in the Dpp-Tkv binding rate are shown in Figure 11 (A1)(B1)(C1).This may be established by the way to determine k_{dt}^{-}which leads to constant equilibrium dissociation rate ($K_D = \frac{k_{dt}^{-}}{k_{dt}^{+}}$) and binding affinity. Moreover, we computed the sensitivity of the system to specific values of the diffusion coefficient. To this end, we varied the diffusion coefficient of Dpp D_{dpp} over twofold from $0.3\mu M^2/s$ to $1.2\mu M^2/s$. It is found that the pattern of pMad is still robust against the change, while an expected change of the decay lengths of Dpp and pMad is observed due to faster or slower effective diffusion. Results of the sensitivity with respect to the diffusion coefficient are provided in Figure 11(A2)(B2)(C2). Finally, we calculated the sensitivity of the system to the Dpp degradation by varying β_{dt} from $1.20 \times 10^{-4}s^{-1}$ to $9.68 \times 10^{-4}s^{-1}$. It is observed that the pattern of pMad is also insensitive to the change of β_{dt} between $1.20 \times 10^{-4}s^{-1}$ to $4.0 \times 10^{-4}s^{-1}$. However, the quantitative measurements differ. The more Dpp degradation, the less decay length of both Dpp and pMad. It may be due to the fact that the more degradation, the less effective transportation. The sensitivity to the change of degradation can be found in Figure 11 (A3)(B3)(C3).

IV Conclusion

Wing imaginal disc of Drosophila is a commonly used model system for the studies of patterning, growth, and scaling. Morphogen Dpp is essential for both patterning and growth in the development of wing disc. Although Dpp is one of the most extensively studied morphogens, there is no current consensus on the mechanisms of how Dpp controls gradient formation, scaling properties, and growth. For instance, experimentally-measured patterns of pMad (an indicator of Dpp signaling activities) and Tkv (Dpp receptor) are quite complicated throughout the whole wing disc, especially around the AP boundary and in the A compartment. How these profiles are formed remains unclear.

In this work, we proposed a baseline mathematical model to investigate the pattern formation of pMad and Tkv gradients with as few players as possible. To this end, some vital accepted experimental observations had been incorporated into our model.[3,12,16,17] It has been shown that our proposed mathematical model of the AP patterning is able to accurately reproduce complex profiles of Tkv and pMad in both anterior and posterior regions of wing disc, as well as overshoots of Hh gradients and its signaling activities.

The above validations give us the confidence to take our model as a digital platform to explore individual roles played by En, Hh, and Dpp in the establishment of complicated profiles of Tkv and pMad. For the purpose, we manipulated individual function terms by adjusting corresponding weight coefficients in the model. It turns out that all En, Hh, Dpp play an essential role in establishing complex experimentally-observed profiles of pMad and Tkv in the whole wing disc. First of all, En dramatically contributes to the sharp jump of pMad across the AP boundary and the highest peak of pMad in the cells abutting to the AP boundary, and its promotion of Tkv also leads to both steeper gradient of pMad and shorter effective range of Dpp in the P compartment than those in the A compartment. Secondly, downregulation of Tkv by Hh in the cells adjacent to the AP boundary highly contributes to the lowest level of Tkv in the

region. It simultaneously prevents the Dpp signaling from interfering and expands the effective range of Dpp gradient. Thirdly, negative modulation of Tkv by Dpp leads to a gradual increase of Tkv distribution toward the peripheries of both A and P compartments. Moreover, the presence of Dpp repression on Tkv determines the position of local and global minimums of pMad and Tkv in the central region which are a few cell diameters away from the AP boundary. Therefore, our computational model supports the essential role of Dpp downregulation on Tkv in shaping the complex Tkv and pMad profiles as proposed previously by experimental researchers,[3,17] although there has been no much experimental confirmations and mechanism studies on it. Furthermore, the present model sheds some light on the underlying mechanism of the negative regulation of Tkv by Dpp. In particular, our model suggests that a suppression strength profile of Tkv by Dpp similar to the pattern of Dpp concentration, instead of that of pMad, can lead to an improved agreement between experimental and numerical results for the complicated distributions of *tkv* expression and pMad.

Finally, the sensitivity of the computational system is examined with respect to specific choices of key parameters including the Dpp-Tkv binding rate, the effective diffusion coefficient of Dpp, and the Dpp degradation. It is found that the pattern of pMad is insensitive to the changes of those core parameters within a certain range. Therefore, our results and conclusions are robust against particular choices of parameter values. For the future work, an improved model to study how Dpp represses its own receptor Tkv is under investigation by including more downstream intracellular players. Hopefully, a better understanding of why the Tkv levels climb sharply in the periphery region can be achieved. Secondly, it is expected that our proposed baseline model can serve as a starting point for further studies on other players, such as Gbb, Sax, Pent and Dally, and for theoretically exploring their roles in the AP patterning and growth. By doing so, more insights can be obtained about the underlying mechanisms of patterning, growth, and scaling in the whole Drosophila wing disc.

Acknowledgments

Authors give special thanks to Dr. Hans G Othmer of the University of Minnesota for past invaluable supports and inspiring discussions which led to authors' intense interest in the subject of Drosophila wing imaginal disc. Also, the authors would like to thank the anonymous reviewers for their constructive comments and suggestions to improve the quality of the paper.

V Appendix

V.A Proof that gene *tkv* expression level is proportional to the level of total Tkv proteins

If we have gene *tkv* in the model system, all regulations (positive and negative) of Tkv will be upon the gene *tkv*. Then we may have three equations as the following to describe the levels of gene *tkv* expression [*tkv*], free Tkv protein $[Tkv]$) and Bound Tkv protein$[\overline{DT}]$, respectively :

$$\frac{\partial[tkv]}{\partial t} = \alpha'_{tkv} + (1-a(x))\alpha'_{entkv} - \frac{r'_{dpptkv}[Dpp]}{[Dpp]_{max}} - \frac{r'_{hhtkv}(\frac{[\overline{HP}]}{[Ptc]})^n}{(M_{tkv})^n + (\frac{[\overline{HP}]}{[Ptc]})^n} - \beta'_{tkv}[tkv] \tag{9}$$

$$\frac{\partial[Tkv]}{\partial t} = T_{tkv}[tkv] - k^+_{dt}[Dpp][Tkv] + k^-_{dt}[\overline{DT}] - \beta_{tkv}[Tkv] \tag{10}$$

$$\frac{\partial[\overline{DT}]}{\partial t} = k^+_{dt}[Dpp][Tkv] - k^-_{dt}[\overline{DT}] - \beta_{dt}[\overline{DT}] \tag{11}$$

Where $\alpha'_{tkv} = \alpha_{tkv}/T_{tkv}, \alpha'_{entkv} = \alpha_{entkv}/T_{tkv}, r'_{hhtkv} = r_{hhtkv}/T_{tkv}$ are all regulation rates, and T_{tkv} represents the translation rate from gene *tkv* to free protein Tkv. Addition of Equation (10) and Equation (7) leads to the following equation for the rate of change of total Tkv proteins.

$$\frac{\partial[Tkv]}{\partial t} = T_{tkv}[tkv] - \beta_{tkv}[Tkv] - \beta_{dt}[\overline{DT}] \tag{12}$$

When $\beta_{tkv} \approx \beta_{dt}$ considering that the degradation of Dpp is most likely receptor driven,[25,26] at the equilibrium state we have

$$[tkv] = \frac{\beta_{tkv}}{T_{tkv}}([\overline{DT}] + [Tkv])$$

The above process shows that it is reasonable to assume that the gene *tkv* expression level is proportional to the level of total Tkv protein which consists of $[\overline{DT}]$ and $[Tkv]$.

V.B Parameters estimation

A base set of all parameter values was chosen for our computation and reported in Table (1) and Table (2). A major portion of detailed estimate processes, related supporting literature is described here. In particular, some of them for core parameter values are described in the following:

V.B.1 Parameters involved in the Hh module

Since our Hh module was modified from a previous model by Nahmad et al,[5] most parameter values used in Equations (1), (3) and (4) were taken from their sound estimates. Readers can refer to the paper and its supporting material for biological references. However, parameter values involved in Equation (2) have to be re-estimated due to our model modifications. Detailed estimation is given as follow: In the Nahmad's model, both gene *ptc* and protein Ptc are included and modeled as

$$\frac{\partial[ptc]}{\partial t} = a(x)\alpha_{ptc0} + \alpha_{ptc}\frac{[Signal]^p}{(M_{ptc})^p + [Signal]^p} - \beta_{ptc}[ptc] \tag{13}$$

$$\frac{\partial[Ptc]}{\partial t} = T_{Ptc}[ptc] - k^+_{hp}[Hh][Ptc] - \beta_{Ptc}[Ptc] \tag{14}$$

where α_{ptc0} and α_{ptc} are the transcription rate and maximal activation rate for ptc, respectively. T_{Ptc} is for the Ptc translation rate. At steady state, the concentration of ptc is

$$[ptc] = a(x)\frac{\alpha_{ptc0}}{\beta_{ptc}} + \frac{\alpha_{ptc}}{\beta_{ptc}}\frac{[Signal]^p}{(M_{ptc})^p + [Signal]^p} \tag{15}$$

Then plugging the concentration expression of ptc (15) into equation (14) leads to an equation for the dynamic of protein Ptc:

$$\frac{\partial[Ptc]}{\partial t} = a(x)T_{Ptc}\alpha_{ptc0}/\beta_{ptc} + T_{Ptc}\alpha_{ptc}/\beta_{ptc}\frac{[Signal]^p}{(M_{ptc})^p + [Signal]^p} - k^+_{hp}[Hh][Ptc] - \beta_{Ptc}[Ptc] \quad (16)$$

We set $\alpha_{Ptc} = \frac{T_{Ptc}\alpha_{ptc0}}{\beta_{ptc}}$, $M_{Ptc} = M_{ptc}$ and $\alpha_{sigptc} = \frac{T_{Ptc}\alpha_{ptc}}{\beta_{ptc}}$ so that Equation (16) are the same as the equation (2). Here parameter values $T_{Ptc}, \alpha_{ptc0}, \beta_{ptc}, M_{ptc}, \alpha_{ptc}, \beta_{ptc}$ comes from the Nahmad's paper. Finally, all of basic parameter values for the Hh module used in our simulations are listed in Table 1.

V.B.2 Parameters in the Dpp module

Parameter values in the Dpp signaling module were either extracted from the literature or estimated according to empirical or experimental measurements. First of all, some core parameters were decided and their values were determined first. Then most remaining parameters were calculated either from the literature or based on a specific relationship between some of the core parameters and individual parameters. Those relationships are derived according to particular acceptable experimental measurements at a steady state such as Dpp decay length measured by Kicheva et al.[23] Finally, a base set of all parameter values was chosen for our computation and reported in Table (2). Their detailed estimate processes and related supporting literature are described as follows:

Diffusion Coefficients A simple formulation can provide a starting point for the diffusion estimation of mobile species in terms of the molecular weight M, temperature T and solution viscosity μ[36]

$$D = 8.34 * 10^{-8}(\frac{T}{\mu M^{1/3}}) \quad cm^2 s^{-1} \quad (17)$$

With equation (17), one can calculate that the green fluorescent protein (GFP), a 238 amino acid and 27 KDa protein, has a sound diffusion coefficient of $85\mu m^2 s^{-1}$ in water by assuming 1cP for the viscosity of water and 298 K for temperature T. However, the cytoplasm is considerably more viscous than water under the same temperature, roughly by a factor of 10. As such, Lander et al. used $10\mu m^2 s^{-1}$ for the Dpp diffusion coefficient in their numerical simulations.[9] Moreover, if the adjustment for tissue tortuosity is taken into consideration, the diffusion can be 4-5 fold lower than that without the tissue tortuosity.[9] Furthermore, when it involves impacts from the binding to immobile extracellular matrix molecules, binding to membrane receptors, and endocytosis, the restricted diffusion can be further slower. Therefore, by considering diffusion and degradation of Dpp only in a wing disc and aided with experimental measurements, Kicheva et al. estimated the effective diffusion coefficient of GFP-Dpp to be $0.1 \pm 0.05\mu m^2 s^{-1}$.[23] Since the binding to membrane receptors is explicitly considered in our model, our effective diffusion coefficients should be bigger than $0.1\mu m^2 s^{-1}$. Based on the above considerations, $0.5\mu m^2 s^{-1}$ is set as a base value in our computations.

Degradation rates It was biochemically measured that the extracellular Dpp molecules in the Drosophila wing discs are degraded almost entirely within 3 hours.[27] As such, the degradation rate of Dpp should be greater than $10^{-4} s^{-1}$. With the aid of a computational model, Kicheva et al. estimated that Dpp was degraded at a rate $\beta_{dt} = 2.52 \times 10^{-4} s^{-1} \pm 1.29 \times 10^{-4} s^{-1}$ which corresponds to a GFP-Dpp half-life of about 45 minutes which is consistent with the turnover time of Dpp in the developing wing.[23] In the present work and others,[25] it is assumed that Dpp degradation is receptor-driven. Because of it, the degradation rate of Dpp-Tkv complex should be comparable to the degradation rate of Dpp. Therefore, we set $\beta_{dt} = 2.52 \times 10^{-4} s^{-1}$ as its base value which is similar to what were used in other numerical work.[9,25] In addition, we set $\beta_{tkv} = \beta_{dt} = 2.52 \times 10^{-4} s^{-1}$ assuming that bound and unbound Tkv have the same degradation rate.

Kinetic binding parameters For the binding affinity k^+_{dt}, we set $0.1\mu M^{-1} s^{-1}$ as its base value. $0.1\mu M^{-1} s^{-1}$ was estimated by Lander et al for the Dpp association rate to obtain an acceptable maximum of receptors per cell.[9] It was also used by Nahmad et al for the association of Hh and its receptor Ptc.[5]

Moreover, k_{dt}^{-} is estimated in a way that the numerical decay length of Dpp can be consistent with the experimental measurement by Kicheva et al.[23] The measured decay length is $20.2 \pm 5.7 \mu m$ in the P compartment. The following is our computational process of k_{dt}^{-}: First of all, considering that the concentration of a measured functional GFP-Dpp in the Kicheva's work actually equals to the summation of the concentrations of free Dpp and its complex $\overline{DT}$ in our work, we combined Equations (5) and (7) to have

$$\frac{\partial[Dpp + \overline{DT}]}{\partial t} = D_{dpp}\frac{\partial^2[Dpp]}{x^2} - \beta_{dt}[\overline{DT}] \tag{18}$$

According to Equation (7), at equilibrium state

$$\begin{aligned}[\overline{DT}] &= \frac{k_{dt}^{+}}{k_{dt}^{-} + \beta_{dt}}[Dpp][Tkv] \\ &\approx C_{dt}[Dpp] \end{aligned} \tag{19}$$

where $C_{dt} = \frac{k_{dt}^{+}}{k_{dt}^{-}+\beta_{dt}}[Tkv]_{max}$. Here we assumed that in the P compartment where the decay length was experimentally-measured, the concentration of Tkv can be roughly regarded as a constant. The constant is similar to the maximum receptor level of Tkv $[Tkv]_{max}$ in the A compartment which is estimated in next paragraph. This assumption is supported by experimental observations that Tkv levels does not change dramatically in the P compartment and that the basal Tkv level in the P compartment is comparable to the maximum level of Tkv in the A compartment (See Figure 2 (D)). Then plugging (19) into Equation (18) yields

$$\frac{\partial[Dpp]}{\partial t} = \frac{D_{dpp}}{1 + C_{dt}}\frac{\partial^2[Dpp]}{x^2} - \frac{\beta_{dt}C_{dt}}{1 + C_{dt}}[Dpp] \tag{20}$$

This leads to a formula of decay length γ of Dpp

$$\gamma = \sqrt{\frac{D_{dpp}}{\beta_{dt}C_{dt}}} \tag{21}$$

From equation (21), k_{dt}^{-} is calculated as

$$k_{dt}^{-} = \frac{\gamma^2\beta_{dt}k_{dt}^{+}[Tkv]_{max}}{D_{dpp}} \tag{22}$$

By using the values of $\beta_{dt}, k_{dt}^{+}, [Tkv]_{max}, D_{dpp}$ and experimentally-measured $\gamma = 20.2\ \mu m$, one has $k_{dt}^{-} \approx 0.0067\ s^{-1}$.

Maximum levels of Dpp and receptor Tkv It was measured by Kicheva et al[23] that the maxmum level of Dpp at the source boundary is $\rho = 4379 \pm 1741$ molecules per cell. Based on this measurement, we obtained $[Dpp]_{max} \approx 0.90 \mu M$ by a conversion formula $[Dpp] = \frac{\rho}{VN_A}$ in which N_A is Avogadro constant 6.022×10^{23} and $V \approx \frac{4}{3}\pi(2.5/2)^3 = 8.18 \mu m^3$. Moreover, the maximum receptor level of Tkv in the wing disc system was estimated at 1600 molecules per cells.[5,9] With the same unit conversion, it is equivalent to $0.34 \mu M$ which was taken as our $[Tkv]_{max}$.

Maximal activation rate At the place where the maximum level of Dpp occurs, the net production of Dpp should be maximized, and the diffusion effects can be ignored. As such, from the equation (5) at the steady state, one has in the position of maximum Dpp level:

$$\begin{aligned}\alpha_{dpp} &= k_{dt}^{+}[Dpp]_{max}[Tkv] - k_{dt}^{-}[DT] \\ &= k_{dt}^{+}[Dpp]_{max}[Tkv] - \frac{k_{dt}^{-}k_{dt}^{+}}{k_{dt}^{-} + \beta_{dt}}[Dpp]_{max}[Tkv] \qquad (23) \\ &= \frac{k_{dt}^{+}\beta_{dt}}{(k_{dt}^{-} + \beta_{dt})}[Dpp]_{max}[Tkv] \qquad (24)\end{aligned}$$

Moreover, we set the concentration $[Tkv] = c_l[Tkv]_{max}$ at the position of maximized Dpp. Here c_l is a small number (we set it equal to 0.2 in our computation) since the Tkv level is much lower in the position than the maximum value.[3] Plugging the related parameter values into Equation (23) gives us $\alpha_{dpp} = 2 \times 10^{-4} \mu M s^{-1}$.

To estimate the ubiquitous activation rate α_{tkv}, we chose a place far away from the AP boundary in the A compartment to get rid of Hh and Dpp repressions, En upregulation and interactions with Dpp. Then at steady state, Equation (6) becomes

$$\alpha_{tkv} = \beta_{Tkv}[Tkv]_{max}$$

In addition, α_{en}, which is used to model the En upregulation of the Tkv,[3] is set as $\alpha_{en} = \frac{4}{5}\alpha_{tkv}$. Coefficient $\frac{4}{5}$ was approximated according to the experimentally measured profile (see Figure 2 (D)) in which the maximum level of Tkv in the P compartment is much higher than the maximum level in the A compartment but less than twofold. Finally, through numerical trials, we set Hh repression rate $r_{hhtkv} = \frac{2}{5}\alpha_{tkv}$ and $r_{dpptkv} = 2\alpha_{tkv}$ to make $[Tkv]$ very low in the Hh signaling cells as shown in experimental profiles.[3]

Other Hill function related parameters We set $d = p = 3$, $n = s = 6.8$ and $M_{tkv} = M_{signal} = 2.135$ as used in the Nahmad's model[5] for the Hh signaling network. Moreover, the half maximal activation parameter M_{dpp} should be smaller than M_{Ptc} since the expression of gene *dpp* is induced with a much lower threshold than gene *ptc*.[3,28] Here $M_{dpp} = 0.05\mu M < M_{Ptc} = 0.14\mu M$ in our computation.

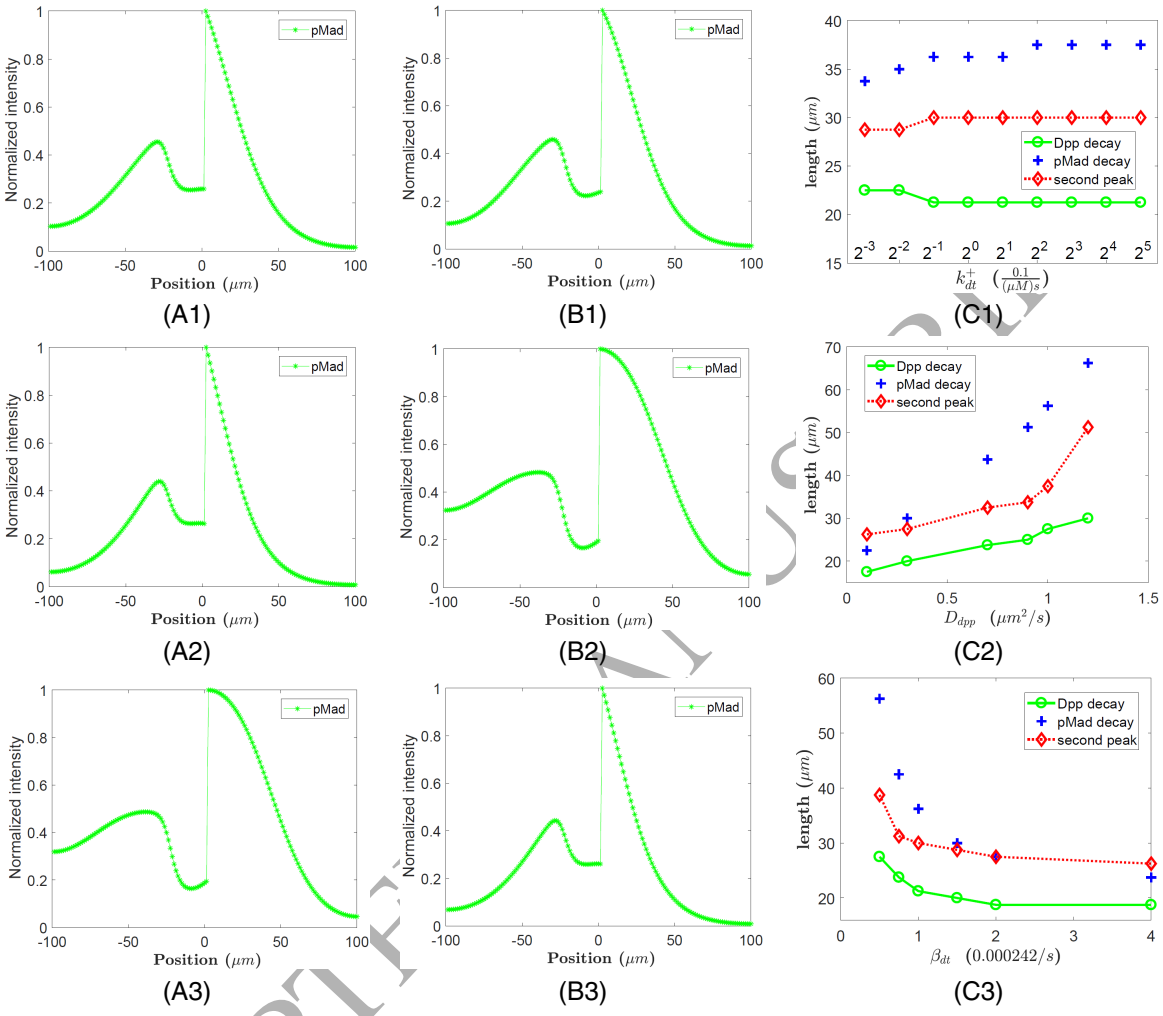

Figure 11: **Sensitivity of the system to the receptor/ligand binding rate k_{dt}^{+} (A1,B1,C1),** D_{dpp} (A2,B2,C2), and β_{dt} (A3,B3,C3). (A1) The pMad profile when $k_{dt}^{+} = 0.02\mu M^{-1}s^{-1}$. (B1) The pMad profile when $k_{dt}^{+} = 3.2\mu M^{-1}s^{-1}$. (C1) Plots of Dpp decay length, pMad decay length and the distance of second peak of pMad from the AP boundary with the changes of k_{dt}^{+}. k_{dt}^{+} varies over eightfold from $0.02M^{-1}s^{-1}$to $3.2M^{-1}s^{-1}$. It turns out that with the value of k_{dt}^{+} changing over eightfold, not only the pattern of pMad level is maintained, but also the quantitative measurements of decay length of pMad and the position of its second peak. Moreover, (A2) The pMad profile when $D_{dpp} = 0.3\mu M^2/s$. (B2) The pMad profile when $D_{dpp} = 1.0\mu M^2/s$. (C3) Plots of Dpp decay length, pMad decay length and the distance of second peak of pMad from the AP boundary with the changes of D_{dpp}. D_{dpp} is varied over twofold from $0.3\mu M^2/s$ to $1.2\mu M^2/s$. It is seen that the pattern of pMad is still robust against the change of D_{dpp}, while an expected change of the decay lengths of Dpp and pMad is observed due to much faster or slower effective diffusion. In addition, (A3) The pMad profile when $\beta_{dt} = 1.21 \times 10^{-4}s^{-1}$. (B3) The pMad profile when $\beta_{dt} = 4.0 \times 10^{-4}s^{-1}$. (C3) Plots of Dpp decay length, pMad decay length and the distance of second peak of pMad from the AP boundary with the changes of β_{dt}. β_{dt} varies over threefold from $1.21 \times 10^{-4}s^{-1}$ to $9.68 \times 10^{-4}s^{-1}$. It is found that the pattern of pMad is insensitive to the change of β_{dt} value between $1.21 \times 10^{-4}s^{-1}$ to $4 \times 10^{-4}s^{-1}$, while the decay lengths of Dpp and pMad and the distance of second peak from the AP boundary decreases with the increase of degradation rate. This is due to the fact that the more degradation, the less effective transportation.

Literature cited

[1] Fisun Hamaratoglu, Markus Affolter, and George Pyrowolakis. Dpp/bmp signaling in flies: from molecules to biology. In *Seminars in cell & developmental biology*, volume 32, pages 128–136. Elsevier, 2014.

[2] Udai Bhan Pandey and Charles D Nichols. Human disease models in drosophila melanogaster and the role of the fly in therapeutic drug discovery. *Pharmacological reviews*, 63(2):411–436, 2011.

[3] T. Tabata and Y. Takei. Morphogens, their identification and regulation. *Development*, 131(4):703–12, 2004.

[4] David M Umulis and Hans G Othmer. The role of mathematical models in understanding pattern formation in developmental biology. *Bulletin of mathematical biology*, 77(5):817–845, 2015.

[5] Marcos Nahmad and Angelike Stathopoulos. Dynamic interpretation of hedgehog signaling in the drosophila wing disc. *PLoS biology*, 7(9):e1000202, 2009.

[6] Andreu Casali and Gary Struhl. Reading the hedgehog morphogen gradient by measuring the ratio of bound to unbound patched protein. *Nature*, 431(7004):76–80, 2004.

[7] Natalie K Gordon and Richard Gordon. *Embryogenesis Explained*. World Scientific, 2017.

[8] Natalie K Gordon and Richard Gordon. The organelle of differentiation in embryos: the cell state splitter. *Theoretical Biology and Medical Modelling*, 13(1):11, 2016.

[9] A. D. Lander, Q. Nie, and F. Y. Wan. Do morphogen gradients arise by diffusion? *Dev Cell*, 2(6):785–96, 2002.

[10] Shaohua Zhou, Wing-Cheong Lo, Jeffrey L Suhalim, Michelle A Digman, Enrico Gratton, Qing Nie, and Arthur D Lander. Free extracellular diffusion creates the dpp morphogen gradient of the drosophila wing disc. *Current Biology*, 22(8):668–675, 2012.

[11] Simon Restrepo, Jeremiah J Zartman, and Konrad Basler. Coordination of patterning and growth by the morphogen dpp. *Current Biology*, 24(6):R245–R255, 2014.

[12] H. Tanimoto, S. Itoh, P. ten Dijke, and T. Tabata. Hedgehog creates a gradient of DPP activity in Drosophila wing imaginal discs. *Mol Cell*, 5(1):59–71, January 2000.

[13] G. Schwank, S. Restrepo, and K. Basler. Growth regulation by Dpp: an essential role for Brinker and a non-essential role for graded signaling levels. *Development*, 135(24):4003, 2008.

[14] Richard Burke and Konrad Basler. Dpp receptors are autonomously required for cell proliferation in the entire developing drosophila wing. *Development*, 122(7):2261–2269, 1996.

[15] D. Ben-Zvi, G. Pyrowolakis, Naama Barkai, and B. Shilo1. Expansion-repression mechanism for scaling the dpp activation gradient in drosophila wing imaginal discs, 2011.

[16] Y. Funakoshi, M. Minami, and T. Tabata. mtv shapes the activity gradient of the Dpp morphogen through regulation of thickveins. *Development*, 128(1):67, 2001.

[17] T. Lecuit and S. M. Cohen. Dpp receptor levels contribute to shaping the dpp morphogen gradient in the *Drosophila* wing imaginal disc. *Development*, 125:4901–4907, 1998.

[18] E. Bangi and K. Wharton. Dpp and gbb exhibit different effective ranges in the establishment of the BMP activity gradient critical for drosophila wing patterning. *Dev Biol*, 295(1):178–93, 2006.

[19] Robin Vuilleumier, Alexander Springhorn, Lucy Patterson, Stefanie Koidl, Matthias Hammerschmidt, Markus Affolter, and George Pyrowolakis. Control of dpp morphogen signalling by a secreted feedback regulator. *Nature cell biology*, 12(6):611–617, 2010.

[20] M. Fujise, S. Takeo, K. Kamimura, T. Matsuo, T. Aigaki, S. Izumi, and H. Nakato. Dally regulates dpp morphogen gradient formation in the *Drosophila* wing. *Development*, 130(8):1515–22, 2003.

[21] David M Umulis. Analysis of dynamic morphogen scale invariance. *Journal of The Royal Society Interface*, pages rsif–2009, 2009.

[22] O Wartlick and M González-Gaitán. The missing link: implementation of morphogenetic growth control on the cellular and molecular level. *Current opinion in genetics & development*, 21(6):690–695, 2011.

[23] Anna Kicheva, Periklis Pantazis, Tobias Bollenbach, Yannis Kalaidzidis, Thomas Bittig, Frank Julicher, and Marcos Gonzalez-Gaitan. Kinetics of morphogen gradient formation. *Science*, 315(5811):521–525, January 2007.

[24] David J. Irons, Alexandre Wojcinski, Bruno Glise, and Nicholas A.M. Monk. Robustness of positional specification by the Hedgehog morphogen gradient. *Developmental Biology*, 342:180–193, 2010.

[25] A. D. Lander, Q. Nie, and F. Y. M. Wan. Spatially distributed morphogen production and morphogen gradient formation. *Mathematical biosciences and engineering*, unknown(2):239–262, 2005.

[26] C. M. Mizutani, Q. Nie, F. Y. Wan, Y. T. Zhang, P. Vilmos, R. Sousa-Neves, E. Bier, J. L. Marsh, and A. D. Lander. Formation of the BMP activity gradient in the Drosophila embryo. *Dev. Cell*, 8(6):915–24, 2005.

[27] A. U. Teleman and S. M. Cohen. Dpp gradient formation in the *drosophila* wing imaginal disc. *Cell*, 103(6):971–980, December 2000.

[28] Katie L Ayers, Armel Gallet, Laurence Staccini-Lavenant, and Pascal P Thérond. The long-range activity of hedgehog is regulated in the apical extracellular space by the glypican dally and the hydrolase notum. *Developmental cell*, 18(4):605–620, 2010.

[29] Maura Strigini and Stephen M. Cohen. A hedgehog activity gradient contributes to AP axial patterning of the drosophila wing. *Development*, 124:4697–4705, 1997.

[30] K. Shimizu and J. B. Gurdon. A quantitative analysis of signal transduction from activin receptor to nucleus and its relevance to morphogen gradient interpretation. *Proc Natl Acad Sci*, 96(12):6791–9796, 1999.

[31] Zhan Chen. The formation of the thickveins (tkv) gradient in drosophila wing discs: A theoretical study. *Journal of Theoretical Biology*, 474:25–41, 2019.

[32] Katie L Ayers, Armel Gallet, Laurence Staccini-Lavenant, and Pascal P Thérond. The long-range activity of hedgehog is regulated in the apical extracellular space by the glypican dally and the hydrolase notum. *Developmental cell*, 18(4):605–620, 2010.

[33] Tobias Bollenbach, Periklis Pantazis, Anna Kicheva, Christian Bökel, Marcos González-Gaitán, and Frank Jülicher. Precision of the dpp gradient. *Development*, 135(6):1137–1146, 2008.

[34] D. M. Umulis, M. Serpe, M. B. O'Connor, and H. G. Othmer. Robust, bistable patterning of the dorsal surface of the drosophila embryo. *Proc Natl Acad Sci U S A*, 103(31):11613–8, August 1 2006.

[35] David M Umulis, Mihaela Serpe, Michael B OConnor, and Hans G Othmer. Robust, bistable patterning of the dorsal surface of the drosophila embryo. *Proceedings of the National Academy of Sciences*, 103(31):11613–11618, 2006.

[36] M.E. Young, P.A. Carroad, and R.L. Bell. Estimation of diffusion coefficients of proteins. *Biotechnol.Bioeng*, 22, 1980.